Tampere University

Ines Calado Baptista

EFFICIENCY AND ROBUSTNESS TO NONOPTIMAL TEMPERATURES OF NUCLEOID EXCLUSION PROCESSES IN *ESCHERICHIA COLI*

Faculty of Medicine and Health Technology
Master's Thesis
July 2019

ABSTRACT

Ines Calado Baptista: Efficiency and Robustness to Nonoptimal Temperatures of Nucleoid Exclusion Processes in *Escherichia coli*
Master's Thesis
Tampere University
Master's Degree Program: Erasmus Exchange Student
July 2019

Prokaryotic organisms, such as *Escherichia coli*, lack internal wall. Nevertheless, they have internal spatial organization, which is a critical requirement for the proper functioning of several cellular processes. One of the internal structures that is crucial for the emergence and maintenance of such organization is the nucleoid. With a higher density than the cytoplasm, the nucleoid is able to segregate different macromolecules — such as protein aggregates and chemotaxis clusters — to the cell poles, while also placing structures, such as the Z-ring, between recently replicated nucleoids during cell division. In this regard, for a cell population to thrive in fluctuating environments, these cellular processes need not only to be efficient in optimal conditions, but also robust to nonoptimal conditions.

Here, we study the efficiency of the processes of segregation of protein aggregates, polarization of chemotaxis network, and Z-ring positioning at midcell and relate it with the nucleoid's morphology. In order to evaluate their robustness to nonoptimal conditions, we also study the effects of temperature shifts on the nucleoid(s) morphology, and how this then affects the efficiency of these biophysical processes.

For this, we collected confocal microscopy images of populations of cells with fluorescently tagged protein aggregates, protein clusters composing the chemotaxis networks, and FtsZ-proteins composing Z-rings, at different temperatures. In addition, we also stained the nucleoids of these cells.

From the analysis of the data collected from the images, we found that, for each temperature condition, the spatial distribution of the cellular components observed is consistent with the nucleoid's volume exclusion effect. Furthermore, we found that the nucleoid's length along the major cell axis is correlated with the kurtosis of the spatial distribution of protein aggregates and chemotaxis clusters along that axis. Similarly, the distribution of distances between replicated nucleoids (prior to cell division) along the major cell axis is correlated with the kurtosis of the spatial distribution of Z-rings along that axis. Finally, we found a negative correlation between the efficiency of these spatial placement processes at optimal temperatures and their robustness to nonoptimal temperatures, indicating a trade-off between these features.

Overall, these results suggest that the robustness of the morphological features of the nucleoid to temperature shifts contribute to the adaptability of *E. coli* to non-optimal temperatures.

Keywords: Nucleoid exclusion, efficiency and robustness, cell division, protein aggregates, chemotaxis

PREFACE

This thesis and the five years preceding it were only possible due to the support of many people, some of which I would like to express my gratitude:

First, I would like to thank both of my supervisors. To Professor José Manuel Fonseca for allowing me to have this opportunity and for supporting me every step of this process. To Professor Andre Sanches Ribeiro for accepting me into the LBD group, for teaching me how the academic field works and for being a constant example on the hard work and dedication that are necessary to thrive in the research world.

To the LBD lab, for welcoming me to the group and helping me along the way. To Bilena for all the help and advice given along these past months. To Cristina for all the advice that eased my settling in and helped me to get to know and enjoy the Finnish lifestyle. To Mohamed for all the knowledge transferred. To Vatsala, for all the support shown since day one. To Vinodh for keeping up the group spirit. To Suchintak for all the interesting discussions. I have learned a lot with you and I am certain I will continue to grow by working with all of you.

To all FCT friends, for the friendship and help you have offered this last five years. I hope all of you will have a successful future and, as me, will be able to look back fondly on our collective misadventures.

To DDN, for being the best support system. To Bruna, for all the advice, pep talks and leading by example. To Leonor, for the non-sense talks, emergency tutoring and inspiring perseverance to pursuit your career. To Marta, for all the laughs shared, all the study sessions that turned to coffee breaks and for being the embodiment of a strong character. To Sara for all the long talks, for being my personal chef and for always showing kindness when facing unkind. I hope these past years have been just the beginning of a lifelong friendship.

Finally, to my family for showing me what a supporting family should be. Words cannot describe how much I admire every one of you. To my sister for supporting me in everything I ever did. I am extremely proud of you. To my parents, for the sacrifice and dedication shown me all my life. I am tremendously grateful that I have you to guide me. Thank you.

Tampere, 23 July 2019

Ines Calado Baptista

CONTENTS

LIST OF FIGURES

LIST OF SYMBOLS AND ABBREVIATIONS

E	Efficiency
CV	Coefficient of variation
D	Distance of a cellular component from midcell
DAPI	4', 6-diamidino-2-phenylindole
DNA	Deoxyribonucleic acid
E. coli	*Escherichia coli*
FP	Fluorescent protein
Fts	Filamenting temperature-sensitive
GFP	Green fluorescent protein
GPL	Gradient path labelling
HupA	Protein Huα
IB	Inclusion bodies
IbpA	Inclusion body protein A
K	Kurtosis
k_B	Boltzmann constant
MCP	Methyl-accepting chemotaxis proteins
mRNA	Messenger RNA
MS2	Bacteriophage MS2 coat protein
n_c	Number of nonoptimal conditions
N_L	Numbers of molecules that were inherited by the left daughter cell
N_R	Numbers of molecules that were inherited by the right daughter cell
oriC	DNA origin of replication
Q_x^2	Level of errors in partitioning
r	Radius of the particle
R	Robustness
RNA	Ribonucleic acid
RNAp	RNA polymerase
SEM	Standard error of the mean
STD	Standard deviation
T	Temperature
ter	DNA replication terminus binding-site
$\langle X \rangle$	Average of a variable X
$\lvert X \rvert$	Absolute value of a variable X
YFP	Yellow fluorescent protein
η	Dynamic viscosity

1. INTRODUCTION

In recent years, technological advances in microscopy techniques and in the engineering of fluorescent proteins [1] have improved the observation of cellular components inside cells, which, in turn, has allowed to further investigate the dynamics of various cellular processes. These studies of prokaryotic organisms have found that, even though they do not have internal organelles (apart from the nucleoid) and their intracellular transport mechanisms are energy-free [2], the cells have a non-random internal organization, differing between cellular components [3]. Moreover, it was also found that the degree of spatial organization of these cellular components affects the success of several of their processes [4]. Some of these processes (for instance, cell division and cell-to cell communication) are crucial for the cell's survival thus, the thriving of the population.

Such studies found that, in *Escherichia coli* (*E. coli*), one of the structures that most influence this intracellular organization is the nucleoid [5]–[8]. Its presence in the central region of the cell causes other macromolecules to be excluded to regions where the nucleoid is not located, due to its higher density than the cytoplasm.

In this organism, as the nucleoid occupies 50 % to 80 % of the cell's volume at the cell center [9] and given the rod shape of the cells, the occlusion caused by the nucleoid places the excluded cellular components at the cell poles. Meanwhile, in cells where the nucleoid has already been replicated but the cell has not yet divided, the two resulting nucleoids force these components to be in the space in between the nucleoids. This is especially important for the formation and placement of the Z-ring, whose building blocks define the location of the division plane.

The recent ability to visualize bacterial populations at the single-cell level, revealed that, even in monoclonal populations, there is cell-to-cell phenotypic variability that is more or less present depending on the cellular process studied, on the environmental conditions the cells are subjected to, and other biophysical properties of the cells [10]–[12]. This diversity is also present on the spatial distributions of cellular components, which affects vital cellular processes. For this reason, much research has been conducted to better comprehend the origins of this diversity, its benefits and drawbacks, and how it is regulated.

In this thesis, we analyzed the spatial organization of three cellular components: the Z-ring, which forms at midcell; the chemotaxis network, which locates at the cell poles; and proteins aggregates, which tend to migrate to the cell poles in the presence of one nucleoid, but also to the cell center, when in the presence of two nucleoids.

For comparing these processes, we have defined and made use of measures of functionality, namely efficiency in optimal conditions and robustness to temperature shifts. We make use of these features to analyze the functioning of these processes and their dependence on the nucleoid's biophysical properties, in particular, its morphology. With this information, we investigate whether the efficiency of the different placement processes and robustness to changing temperatures differs, although relying on the same mechanism.

Here, we first delve the theoretical concepts used to analyze how these processes work and are regulated in *E. coli* cells. Next, we report on relevant past studies of the biophysical properties of *E. coli* regarding the nucleoid exclusion phenomenon, its consequences in the partitioning of cellular components, and other factors that might affect its outcome. Next, we describe the methodology and techniques used to obtain the empirical data and subsequent results here reported and, finally, we present the results, discuss them and, draw conclusions.

2. BIOLOGICAL BACKGROUND

This chapter provides an overview of knowledge from past studies that are used in this thesis. We begin with a brief description of *Escherichia coli*'s biology, including its nucleoid and cytoplasm biophysical features, along with a detailed overview of some of the cell's processes most relevant to our studies, namely, cell division, protein aggregate formation, and the chemotaxis network organization.

2.1 Model organism – *Escherichia coli*

Discovered in 1886 by the pediatrician Theodor Escherich [13], *Escherichia coli* (*E. coli*) has since became one of the most studied organisms in several fields of Biology [3]. The gram-negative, rod-shaped bacterium [2] can be 1.6 μm to 4 μm long and is typically 1.26 μm wide [14] with a similar structure as the bacterial cell depicted in Figure 2.1.

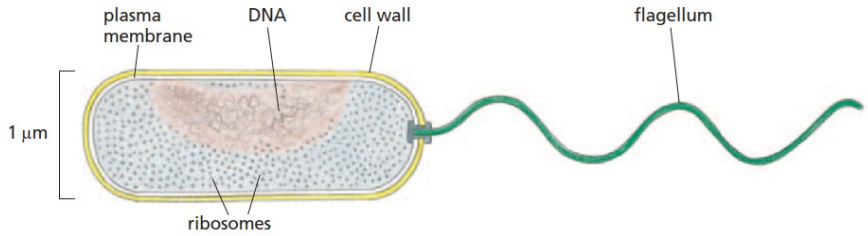

Figure 2.1. *The structure of a common bacterium. Similar to this diagram, the E. coli cell has an inner and outer membrane — separated by the periplasm — as well as a nucleoid, where most of the cell's DNA is concentrated, along with other cellular components that diffuse in the cytoplasm. Unlike the image, E. coli cells have many flagella, which work as propellers to drive the cell forward. Figure adapted from [2].*

This organism ordinarily lives in two distinct habitats, the primary being the colon of warm-blooded animals and the secondary being water, sediment or soil [15]. In both habitats, there are several variables that determine its well-being. Namely, in the primary habitat, the diet, the immune system and the overall physiological state of the host will create a specific environment that can either benefit or harm the cell. In the secondary habitat, factors such as climate and nutrients accessibility greatly affect the cell's odds to thrive [15].

Due to its necessity to endure in these sometimes-harsh living conditions, this prokaryote has evolved characteristics that make it a prime model system to study in laboratory environments. In particular, its fast growth rate, its ability to be anaerobic in oxygen-free environments and its easily manipulated genome are some of the features that make *E. coli* an organism that is easy to maintain, and thus has been used to study cellular processes and bacterial adaptability to environmental changes.

2.1.1 The cytoplasm

In *E. coli*, the cytoplasm is a clear and colorless, gel-like substance that fills the interior of the cell and is composed of an aqueous solution named cytosol [2]. The cytoplasm is often described as a molecular soup, since high concentrations of different macromolecules — ranging from sub-nanometer (inorganic ions and metabolites), to nanometer (proteins), tens and hundreds of nanometers (ribosomes and plasmids) and micrometers (nucleoid) — suspend and diffuse in it.

Due to the high concentration of cellular components in the cytoplasm, there is often an effect of “macromolecular crowding”, which has been shown to induce DNA condensation [16] and influence the dynamics of diffusion of cellular components [17]. This phenomenon is particularly visible in the poles, where some molecules migrated to due to the higher density of the regions where the nucleoid is present.

Since *E. coli* does not have a cytoskeletal system that could aid in the intracellular transport of cellular components, substances in the cell mainly move by diffusion [18], [19], which is the random movement of particles due to thermal agitation. Several factors, such as temperature, the substance’s size and the viscosity of the fluid, can affect the diffusive behavior of a substance. In *E. coli*, there are substances which have a normal and symmetrical diffusion, but there are also substances that have an anomalous and asymmetrical diffusive motion [20]–[23].

The diffusive behavior of a particle can be quantified by the diffusion coefficient *D*, given by the Stokes-Einstein equation [24]:

$$D = \frac{k_B T}{6 \pi \eta r} \ , \tag{2.1}$$

where k_B is the Boltzmann constant, T is temperature, η is the dynamic viscosity of the medium, and r is the radius of the particle. Since the bacterial cytoplasm can have a viscosity up to 10 times higher than water [25], from equation (2.1), one can conclude

that the dynamics of cellular processes may differ from what would be expected otherwise.

2.1.2 The nucleoid

One of the most important internal structures in *E. coli* is the nucleoid. As a prokaryotic organism, *E. coli* does not have nuclear membranes that constrain the bacterial chromosome. Instead, the chromosome and its associated proteins simply concentrate in a middle region in the cytoplasm named the nucleoid [26], as this is location of least energy (due to the curvature of the poles).

The nucleoid is the largest structure in *E. coli*, occupying approximately 75 % of the cellular space [9]. Although occupying this last portion of the cytoplasm, this is only made possible because the chromosome is compacted more than 1,000-fold so as fit inside the cell, using results in a dense core [27]. The degree of compaction depends on various factors, such as medium richness, stage of the cell cycle, and temperature [28].

Prior to cell division, the chromosome must replicate itself and the resulting chromosomes must segregate from midcell, so as to ensure that each daughter cell will inherit one complete nucleoid from the mother cell. Chromosome replication starts from a specific origin of replication site (*oriC*), located near midcell. As depicted in Figure 2.2, multienzyme complexes replicate the DNA — in a left and a right chromosome arm, simultaneously — until they reach a terminus region (*ter*), on the opposite side of the circular chromosome [29]. The *ter* region span is such that it connects the left and right arms, allowing replication to be completed [29]. Next, the newly replicated sister chromosomes are segregated and, even though the process by which it happens is still not entirely understood [30], some studies suggest that segregation might result from physical mechanisms, such as entropy, rather than biological processes [31]. However, entropy is not the only factor responsible for chromosome segregation as it has been shown that the condensation of the nucleoid creates forces that can push sister chromosomes apart, due to the accumulation and release of mechanical stresses in the replicated chromosomes [9]. In addition, the motional bias of chromosome segregation suggests the existence of an active mechanism responsible for this process [32].

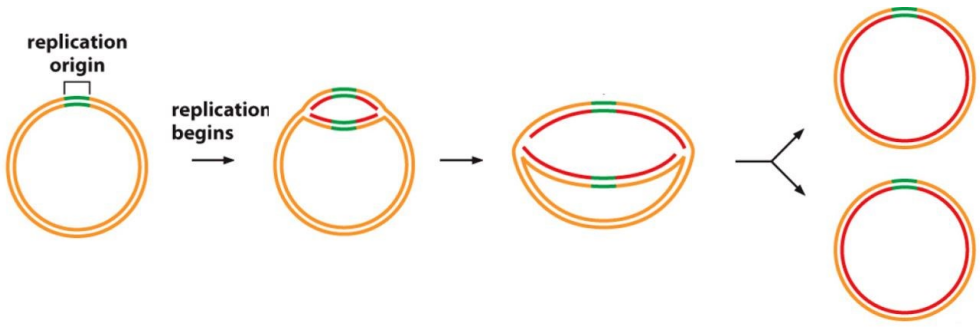

Figure 2.2. *Chromosome replication in E. coli. Replication starts in the replication origin (oriC, represented here as the green region) and proceeds bidirectionally until reaching the terminus region (ter, not represented here), across the oriC region. This is where the left and right arms of each chromosome connect, forming two sister DNA molecules. Figure adapted from [2].*

2.2 Cell cycle and cell division

In its natural environment, *E. coli* lives in changing periods of feast and famine. Therefore, the cell cycle must be meticulously regulated so that the survival of the lineage may be possible in a wide range of conditions.

The rod-shaped *E. coli* cells grow by elongation of the cell wall along the major cell axis, having no significant variation of width between generations [14]. Nevertheless, the cell cycle includes more processes other than elongation, which divide the cell in three periods [33], represented in the scheme in Figure 2.3: (i) period B, the gap phase between the cell's "birth" and initiation of chromosome replication (without essential cell cycle's events); (ii) period C, when the cell, after reaching a certain length, begins to replicate its chromosome; (iii) period D, when cell division occurs, resulting in the "birth" of two daughter cells.

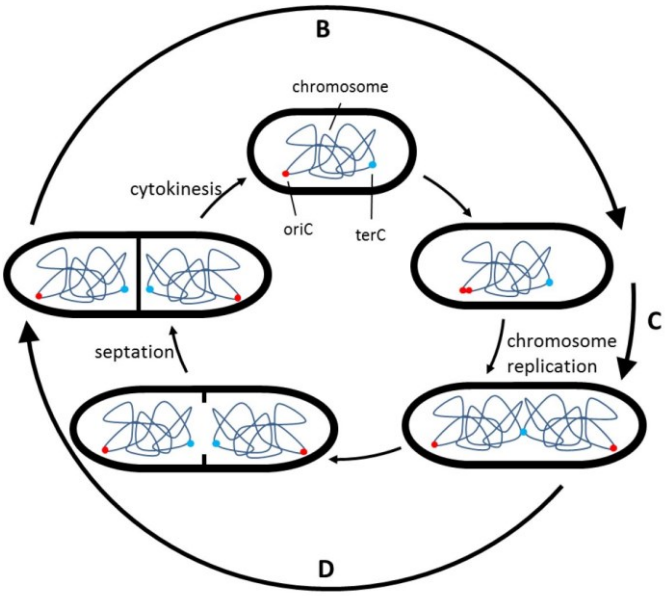

Figure 2.3. *Scheme of the cell cycle of E. coli. Phase C begins with the chromosome replication at the oriC region (red dots) and lasts until the end of the chromosome replication in the ter region (blue dots). Then, phase D starts as the cell prepares to divide and ends only with the cytokinesis of the mother cell into two daughter cells. Phase B is the phase between cell "birth" and the moment before the chromosome begins to replicate. Image adapted from [34].*

When cell division occurs, the mother cell divides in the middle and a new end (pole) is created for each daughter cell. Therefore, as Figure 2.4 depicts, each cell has a pole, termed new pole, which was formed during the division that originated the cell and the other pole, termed old pole, that was inherited from the mother cell [35]. However, since the mother cell also had a new pole and an old pole, the old poles of the two sister cells have different ages. Therefore, the concept of pole age can be defined as the number of divisions the pole "witnessed", that is, the number of times that a pole has participated in a division event without have been created in it.

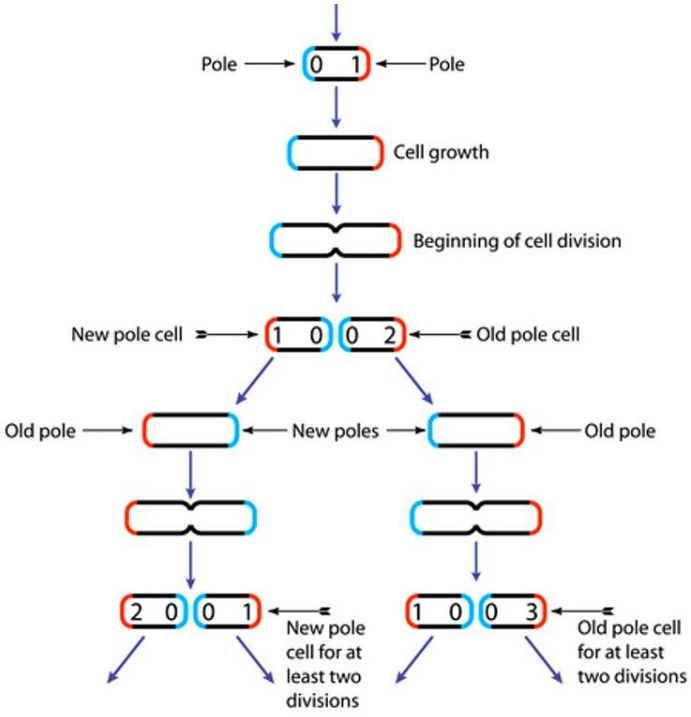

Figure 2.4. *Pole age in E. coli. (A) In each cell, there is a new pole (blue) and an old, inherited pole (red). Each time a cell divides, the daughter cells will have a new pole that was formed in the division process and an old pole that was formed in a former division event. However, since the mother cell had itself a new pole and an old pole, the old poles of the daughter cells will differ in age, with one being younger than the other. In this diagram, the concept of pole age is represented in the numbers in the poles that translate the age of each pole (starting in 0 and increasing one unity each time they a pole "participates" in a division event). Image adapted from [35].*

The crucial step in phase D is cytokinesis, starting from the formation of the divisome in the middle of the mother cell up to the partitioning of the cell into two daughter cells. It is a regulated process that is carried out by an intricate macromolecular apparatus termed divisome [36]. Evidence for this regulation, among other, is the fact that there is a very small variance (i.e. far less than expected by chance) in the positioning of the division point [30].

The divisome is a set of several cytoplasmic, periplasmic and inner membrane proteins that assemble in the division plane [37]. Some of these proteins, such as FtsI and FtsW, are responsible for the construction of the septal apparatus [38], while others, like FtsK, are believed to aid in the chromosome segregation process [39]. Evidence suggests that the most important regulatory protein of the divisome is the FtsZ protein, a tubulin homolog that forms a ring-like structure named Z-ring [40], which is the structure responsible for guiding the septation of the mother cell into two daughter cells [41]. There are three stages during the Z-ring formation [42]: (i) initially, the cell does not have a visible ring and most of the FtsZ proteins are located at one of the poles; (ii)

next, in the open ring state, the FtsZ starts to concentrate in the cell's central region in opposite sites of the minor axis; (iii) finally, in the closed ring state, the FtsZ forms a band at midcell, across the minor cell axis.

In order to produce two daughter cells of equal size, each one with an intact nucleoid, there must be regulatory mechanisms positioning FtsZ at midcell — and, consequently, all of the divisome's components — based on the degree of chromosome segregation (to prevent guillotining DNA). One of these regulators is the MinCDE system, depicted in Figure 2.5, whose component MinC, is an antagonist of FtsZ. MinC inhibits the Z-ring formation by competing with FtsA and ZipA [43] — two proteins essential to the assembly of the Z-ring [44] — to bind to FtsZ and, once bound, weakens the interaction between FtsZ monomers, which prompts Z-ring filament breakage [45].

MinC rapidly oscillates between cell poles due to its interaction with MinD and MinE [46]. First, the peripheral membrane protein MinD recruits MinC to the membrane. Then, MinE separates MinC from MinD and enhances dissociation of MinD from the membrane, sweeping away the MinC and MinD to the opposite pole of the cell, which allows the Z-ring to move to the pole where MinE is [47]. Meanwhile, MinE stays in the cell pole until it no longer detects MinD, at which point it returns to the cytoplasm so that the cycle can restart in the opposite pole [48]. Thus, MinC concentrates at the cell poles and hampers the formation of Z-ring in these regions. Therefore, the midcell — where MinC is minimal — will be the prime location for the Z-ring to form.

Another factor that regulates the placement of the divisome, by preventing it from fragmenting any of the nucleoids when the septum is closing, is nucleoid occlusion, mediated by the SlmA protein [49], also depicted in Figure 2.5. This protein competes with other FtsZ-interacting proteins (necessary for cell division) so that it can bind to the FtsZ [50] and interfere with its polymerization [51]. SlmA binds to specific DNA sequences, located everywhere in the chromosomes, except in the *ter* region [52]. Therefore, the Z-ring formation will only start when the *ter* region is present at midcell, which occurs after the segregation of the vast majority of the chromosome [53] giving time to move the replicated chromosomes away from the division plane before cytokinesis.

While the Min system and nucleoid occlusion are negative regulators, a positive regulator — Ter linkage — guides FtsZ to the division site. This regulator is comprised of the proteins MatP, ZapB and ZapA that join the *ter* region with FtsZ, promoting the assembly of the divisome over this genomic region [54]. As depicted in Figure 2.5, MatP interacts with ZapB [55], which, in turn, interacts with ZapA [56]. Since ZapA interacts with the FtsZ as well [57], it can bridge the *ter* region with the Z-ring. As the Ter linkage

structures tend to form before the Z-ring, this regulatory mechanism is expected to guide the Z-ring towards midcell [54].

Thus, all three mechanisms cooperate to accurately place the Z-ring at midcell and regulate cytokinesis. This ensures that the daughter cells will have equal size and a complete nucleoid each.

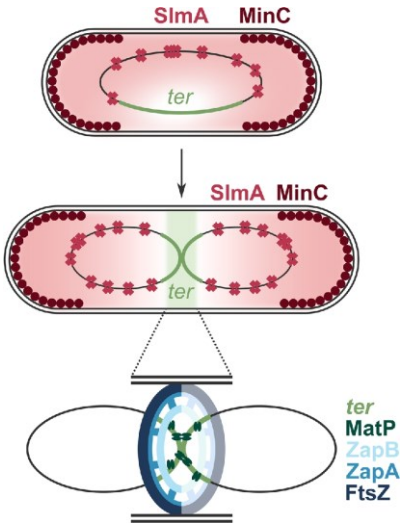

***Figure 2.5**. Control of Z-ring formation in E. coli. The Min system inhibits the formation of the Z-ring close to cell poles, favoring the formation of the Z-ring at midcell. The nucleoid occlusion phenomenon, mediated by the SlmA proteins and the Ter linkage, inhibits divisome assembly in areas occupied by DNA. The areas where the Z-ring is inhibited or stimulated are colored red and green, respectively. Image is adapted from [30].*

The regulation of cell division strives to create two daughter cells that are as equal as possible. Still, many of the cell's substances do not possess any segregation mechanism and partition randomly through the daughter cells, having equal chances of ending up in either one. Their partitioning process is thus well described by a binomial distribution.

Nevertheless, there are small 'errors' in perfect partitioning. While they would not affect the overall functioning of the cell in the case of components that exist in high numbers, in the case of proteins and RNA that have low expression levels [58], they can cause significant differences in the set of components inherited by the daughter cells [3], [59]. Such differences could create phenotypic diversity by influencing the kinetics of various cellular processes, such as transcription, translation and division rate [60]–[62].

2.3 Protein formation and quality control

Proteins are versatile macromolecules that participate in almost every cell process. Each protein is comprised of a sequence of amino acids, which are laid in a specific

order to allow the protein to fold up into a three-dimensional shape. The conformation assembles the protein's functional regions and allows it to interact with other cellular components, either by mechanical or chemical events, which is necessary for the normal functioning of the cell [2].

The generation of proteins entails two steps: transcription and translation. First, the transcription process produces an mRNA from a DNA strand through an RNA polymerase (RNAp) [2]. The RNAp starts the transcription at a promoter region and assembles the mRNA by chain elongation until it reaches a terminator, where it stops transcription and releases the mRNA and the DNA it was created from [63]. Then, or even simultaneously with transcription, the translation process synthesizes a protein from the mRNA, since each set of three nucleoids in the mRNA is recognized by a specific amino acid [63].

The newly made protein still needs to fold into a proper conformation in order to be functional [2]. While some proteins have a sequence of amino acids such that it can fold itself correctly and spontaneously (becoming native proteins), others tend to misfold into nonfunctional conformations [64], which impairs cellular processes.

To address this, the cells developed quality control mechanisms that are responsible for protein homeostasis (proteostasis) [65], represented in Figure 2.6. One of these mechanisms is the aid in proper folding by a particular set of proteins, named chaperones [63]. These assist in *de novo* folding of new proteins or refolding any misfolded proteins [66]. They do so by recognizing exposed hydrophobic regions of non-native proteins and altering the three-dimensional conformation to cover those regions [65]. The cell can also degrade proteins, whether they are misfolded or not. In fact, approximately 20 % of the proteins that are synthesized are degraded, which not only destroys non-native proteins but also ensures the existence of "raw" material for the production of new proteins, allowing the cell to react to changes in its environment [67].

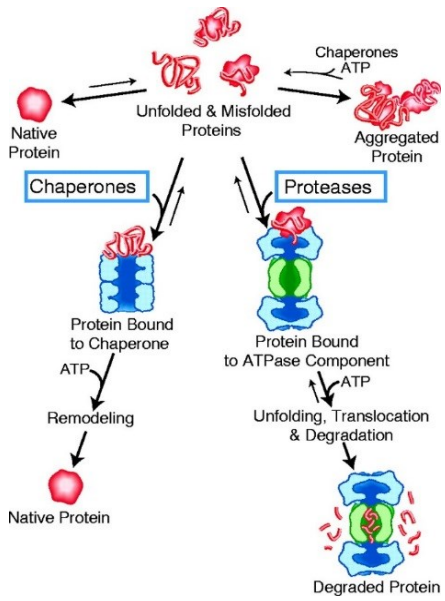

Figure 2.6. *Diagram of the mechanisms of protein quality control. The chaperones catalyze the correct folding of proteins. However, if a protein cannot be refolded properly, the proteases degrade the protein. Finally, if none of the previous mechanisms are available, the nonfunctional proteins will form aggregates. Image adapted from [66].*

Nevertheless, both these mechanisms can fail if the cell is in stressful conditions — either due to antibiotics, nutrient depletion or changes in temperature — by suffering mutations (the proteins of the affected genes keep misfolding) or even by errors in the protein biogenesis process [68]. In these cases, misfolded proteins tend to form clumps to avoid having their hydrophobic regions exposed to the cytosol, forming either amorphous structures or amyloid-like fibrils [69]. These nonfunctional protein aggregates can interact with critical molecules and hamper processes [2]. However, aggregates can be accumulated in inclusion bodies (IBs), which are often found at the cell poles, as depicted in Figure 2.7, and insoluble and metabolically stable [68]. Thus, the aggregation mechanism helps in preserving proteostasis by consigning the misfolded proteins to the IBs, which function as an intracellular deposition site for cellular detoxification [70].

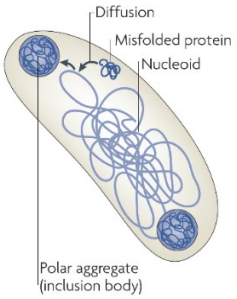

Figure 2.7. *Misfolded proteins deposition in inclusion bodies. These structures are formed mainly at the cell poles. Image adapted from [68].*

2.4 The chemotaxis network

E. coli cells are subject to environmental changes. Consequently, the species has evolved mechanisms to sense these changes and adapt to them. E.g. these cells can move towards or away whether it detects attractants (for instance, a high concentration of nutrients) or repellents (such as noxious chemicals), respectively [71]. These motile responses to extracellular signals are termed chemotactic responses.

E. coli organisms have four to six flagella, each of which protrudes from the cell by a flexible hook, which, in turn, is attached to a protein disc in the inner and outer membranes. This disc is part of a motor that can rotate and turn the flagellum [2]. Due to the "handedness" of the flagella, different directions of rotation will produce different effects on movement. Particularly, if the helical flagella rotate counterclockwise, it will draw all of the flagella into a coherent bundle, causing the bacterium to swim smoothly, as depicted in Figure 2.8 (A). This movement will continue as long as the organism detects an increasing gradient of a chemotactic attractant. However, if the organism does not detect changes in the environment or if it detects an increasing gradient of a chemotactic repellent, one of the motors will rotate clockwise, causing the flagellum attached to separate from the bundle, prompting the cell to tumble without moving forward, as depicted in Figure 2.8 (B) [2]. This mechanism creates a biased random walk towards the better environment, allowing the cell to prosper.

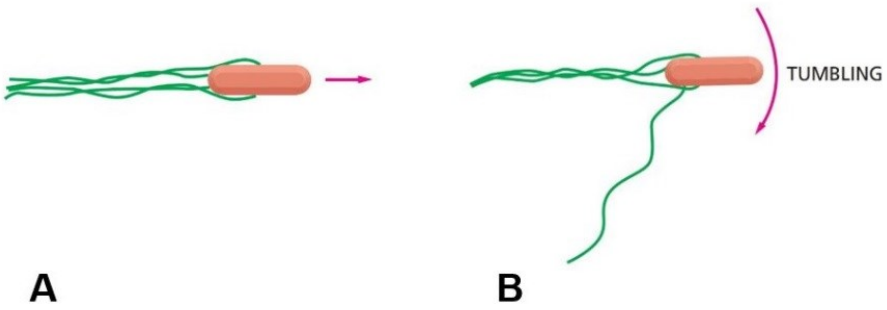

Figure 2.8. *Chemotactic responses of E. coli. (A) If the flagella rotate counterclockwise, they will form a bundle that propel the cell forward through smooth swimming. (B) If one the flagellum rotates clockwise, it will separate from the bundle, causing the cell to tumble. Image adapted from [2].*

Interestingly, *E. coli* senses changes in the environment by making temporal comparisons of the surrounding environment [72]. To be able to compare successive conditions, it must be able to sense the present condition and recall the previous one. This is possible due to chemoreceptors that can both sense various stimuli and remember previous environments through the methylation degree of specific glutamate residues [72]. This last characteristic allows the cell to respond only to increasing or decreasing

gradients rather than constant concentrations, that is, if the high concentration of a chemoreceptor is maintained, the bacterium will eventually be desensitized to the stimulus.

There are five different types of chemoreceptors: Tsr (sensible to serine); Tar (sensible to aspartate and maltose); Tap (sensible to dipeptides); Trg (sensible to ribose and galactose); Aer (sensible to oxygen) [73]. All but the Aer chemoreceptor — which mediates responses in a methylation-free way — are known as methyl-accepting chemotaxis proteins (MCPs) [73].

These chemoreceptors are inserted in the cytoplasmic membrane at the cell poles and are grouped in trimers-of-dimers [74] that organize into intercommunicating clusters [75]. The clustering occurs through an energy-free, self-assembly process named stochastic nucleation [76], which is thought to improve sensitivity, dynamic range, and adaptability of the system [75]. These patches are often circular or ellipsoidal and are stabilized by associating with the histidine kinase CheA via the adaptor protein CheW, forming ternary complexes [77] ranging from ~ 200 – 400 nm in diameter [78], as shown in Figure 2.9 (A).

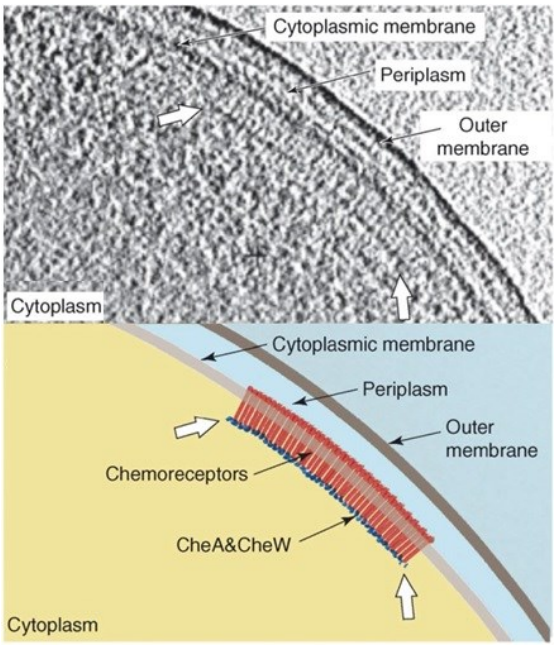

Figure 2.9. *A 5 nm tomographic slice of the region near the pole of an E. coli cell and its schematic. Represented are the inner (cytoplasmic) and outer membrane, the periplasm (light blue) and the cytoplasm (yellow). The white arrows point to the boundaries of the patch of chemoreceptors (represented in red) inserted in the inner membrane, which correspond to a layer of CheA and CheW (blue). Image adapted from [75].*

3. LITERATURE REVIEW

Several studies have been done on the spatial organization of the internal processes of *E. coli*. In this chapter, we look at some which are of importance to this thesis.

3.1 The nucleoid exclusion phenomenon

A recent study [79] used mRNA tagged with MS2-GFP (see section 4.2.2) as a synthetic protein aggregate in order to investigate if the nucleoid could be a source of intracellular organization of cellular components in *E. coli*. The results show that MS2-GFP-mRNA had higher diffusion coefficients in regions with higher nucleoid density, which can be explained by the fact that the nucleoid acts as a crowding agent for the MS2-mRNA and, since it is dynamic via processes such as transcription and replication, changes the MS2-mRNA distribution. It was also observed that the diffusion coefficient at the poles is smaller (particularly at the old pole), which is understandable if we consider the existence of larger macromolecular complexes, such as ribosomes or protein aggregates, which may hamper the movement of the MS2-mRNA complexes.

Thus, the nucleoid exclusion phenomenon along with membrane confinement influence the motion and distribution of molecular complexes in bacterial cells. Therefore, there have been several studies to understand how this phenomenon factors into different processes of the bacterial cell. Here, we examine some of them related to cell division, segregation of protein aggregates and positioning of the chemotaxis network.

3.1.1 Z-ring placement

In optimal conditions, *E. coli*'s cell division is highly regulated to be morphologically symmetric [80] via the division plane formation at midpoint [81]. However, even in monoclonal cell populations, there is some variance in the location of the point of division, causing asymmetric divisions.

A study was recently conducted to investigate *E. coli*'s morphological symmetry in cell division and its robustness to non-optimal conditions [82]. It was found that, even though mild chemical stresses do not affect symmetry in division, changes in temperature from optimal to suboptimal decreases the division symmetry. Particularly, the further the temperature is from the optimal temperature, the more variance there is in the

size of sister cells. Interestingly, asymmetries caused by suboptimal temperatures affect cell division times, as it was found a negative correlation between the division time and the cell size (with larger cells dividing faster than smaller cells). Nevertheless, the opposite does not occur, that is, cells with faster dividing times do not show a higher propensity to divide asymmetrically, regardless of the temperature they were subjected to. This suggests that faster dividing cells do not do so at the cost of symmetry in division. In order to understand the mechanism responsible for the asymmetries that were observed with temperature deviations, the position and size of the nucleoids (prior to cell division) were studied for different temperatures. It was found that, although size does not change significantly, the distance between the nucleoids is minimized at 37 °C, as represented in Figure 3.1. This result can explain the asymmetries found, since the selection of the division plane between the nucleoids was been found to be nearly random. This was further confirmed by the finding that, for all temperature conditions, the cells that divided with higher/lower asymmetry had longer/shorter distances between the nucleoids, respectively. Thus, this study showed that morphological symmetry in cell division changes with temperature, due to the temperature-dependence of the relative distance between nucleoids.

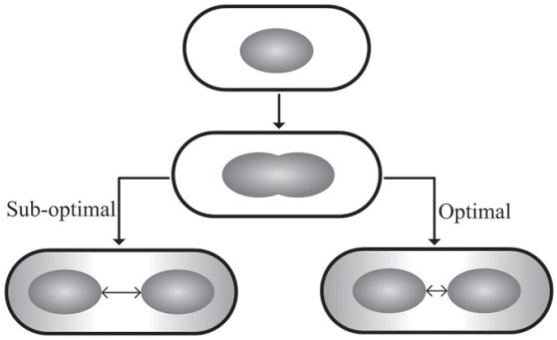

Figure 3.1 *Schematic of the temperature dependence of the relative distance between nucleoids in E. coli. In optimal conditions, the distance between nucleoids is minimal, which minimizes the variance of the placement of the division plane. In suboptimal conditions, the distance between nucleoids increases, resulting in a higher variance in the positioning of the division plane, which, in turn, increases the probability of having an asymmetric division. Image adapted from [82].*

Another study [8] further investigated the effects of temperature on the symmetry in the placement of the Z-ring and if these effects are reversible and/or cumulative. If was found that changes in temperature affect the cells' ability to partition the nucleoids and, more significantly, to reach the close ring state of Z-ring formation. It was also studied how sub-optimal temperatures (24 °C, 30 °C and 40 °C) and critical temperatures (10 °C and 43 °C) affect the distance between nucleoids, the width and density of Z-ring and its displacement from midcell in cells with two nucleoids and a Z-ring in the closed

ring state. At suboptimal conditions, the asymmetry in cell division increases due to a decrease in Z-ring's density — caused be an increase of its width, which, in turn, is caused the increased distance between nucleoids — and an increase in its displacement from midcell. However, the changes in the distance between nucleoids and the consequent Z-ring's displacement from midcell change in a predictable and correlated manner. At critical temperatures, on the other hand, the relation between Z-ring formation/positioning and the position of the nucleoids disappears and the causes for the loss of robustness in the Z-ring formation/positioning may differ for these temperatures. Finally, it was also found that the effects of high temperatures and rich media are cumulative and that the effects of temperature shifting are reversible, suggesting that the placement of the Z-ring is strongly affected by the physical parameters of the environment.

In conclusion, the positioning of the Z-ring is based on the nucleoids size and position. As a result, it is a regulated and robust process.

3.1.2 Segregation of protein aggregates

Unicellular organisms that replicate from symmetric division events do not have a distinct separation between different generations of offspring. Also, provided favorable environment conditions, cell lineages will continue to exist. As such, asymmetrical cell division is expected to be needed for aging [83].

However, it has been identified that, in *E. coli*, some sister cells differ in their division rates [35], which suggests the existence of cellular aging. As described in section 2.2, when a cell divides, each daughter cell will have a new pole formed in the cytokinesis process and an old pole inherited from its mother. However, as the mother cell had poles of different ages, the old poles of the two sister cells will differ in age between them.

A study was recently conducted to investigate if the inheritance of old poles is related to the senescence of *E. coli* cells [35]. By following the growth of a colony of *E. coli* cells at the single cell level, it was possible to observe that cells that inherited old poles more frequently during their ancestry had slower growth rates. Also, the older the pole, the slower was the growth rate of the cell that inherited it. Interestingly, it was also observed that cells that inherited more young poles during their ancestry had increased growth rates (rejuvenation). Thus, there is a relationship between the inheritance of old poles and the aging process. Namely, cells with older poles will have slower growth rates and are at higher risk of not surviving.

Because protein aggregates seem to accumulate at the poles, one study tested the hypothesis that the pole segregation of damaged, nonfunctional proteins may be a physiological reason behind functional asymmetries between sister cells — such as different growth rates — that are related with the aging process [4]. From following cells for several linages, it was found that the first fluorescent IbpA-YFP foci (IbpA is a type of inclusion body that was tagged with the fluorescent protein YFP) in the lineage was either in midcell (28 % incidence), in the new pole (30 % incidence) or in the old pole (31 % incidence). However, since they seldom move from its original location (< 10 % incidence), the location where they first appear in the mother cell was found to determine their position in subsequent generations. As represented in Figure 3.2, this results in the eventual accumulation of damage in the old pole of future daughter cells, regardless of their position in the cell where they first appear. Overall, this results in an accumulation of protein aggregates in the older poles of each cell generation, implying that a few cells of each generation will accumulate damage, while other cells are 'renewed'.

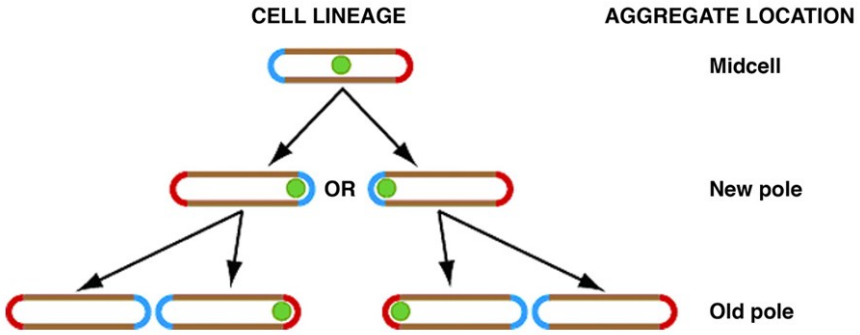

Figure 3.2. *Location of protein aggregates through several divisions. Whatever is the initial location, after several division events, it will be segregated to the pole, if it is unable to move inside the cell. Image adapted from [4].*

The probability of an IbpA-YFP spot appearing in a cell that did not have any foci before was found to be 0.71. However, in cells that already have an IbpA-YFP spot, the probability of appearing a second spot are reduced to 0.037 due to the tendency of misfolded proteins to aggregate. Also, the probability of a cell developing an IbpA-YFP spot when its mother had one and passed it on to its sister cell is 0.69, which is lower than the probability of a cell developing an IbpA-YFP spot when the mother did not have any, which was 0.85. This bias hints for the existence of a damage purification effect, where an inclusion body that is inherited by one sister cell inhibits the other of developing any inclusion bodies. Finally, the study also found that the presence of aggregates in a cell (whatever their position might be) is correlated with a slower growth rate. All of these findings corroborate the hypothesis that it is the protein aggregates that are the cause for aging in *E. coli* cells.

Another study [84] used RNA-MS2-GFP complexes to investigate the spatial kinetics of protein aggregates and their partitioning in cell division. These complexes are first visible soon after the RNA is transcribed, so their initial position is near the cell center (main location of the F plasmids where the RNAs are created [85]) or at the first-quarter or third-quarter position (location of the F plasmids after they replicate [85]). Nevertheless, 95 % of the complexes detected were shifted to the cell poles, where they remained. As a result, in a cell population, the distribution of distances of the complexes (normalized by half of the cell length) is bimodal, with the major peak being located at 0.8 (approximately at midpoint between the nucleoid border and the cell border). It also has a smaller peak at midcell (probably due to the fluorescent RNAs that than remain in that region when being transcribed from the plasmid).

Having identified the *in vivo* localization of aggregated proteins in the older poles and having related their presence with the senescence characteristic of consecutively diminished growth rates, the next step is to study the mechanism responsible for the accumulation of protein aggregates at the poles. Do the aggregates move as a result of biased forces in the cell or do they freely diffuse along the cell until reaching a pole where they tend to remain?

Considering the morphology of *E. coli* cells, whose only organelle is the nucleoid and considering the lack of transport mechanisms, the heterogeneity of the spatial distribution of protein aggregates either results from the presence of the nucleoid at midcell, the shape of the cell and/or the physical properties of the components [9], [23], [60].

One study [5] studied to what extent the nucleoid is involved in the spatial distribution of complexes of unwanted protein aggregates using RNA-MS2-GFP complexes. Similarly to what was found in [4], the initial positions of complexes that appear in a cell that was previously complex-free, are not asymmetrically distributed in the cell. The asymmetries only emerge after cell division, where it is observed a significant bias towards the old pole, as the complexes do not tend to change between poles [4]. However, there a few complexes that can travel between polar regions, which suggests that the retention process has some noise. Interestingly, the standard deviation and mean of the escape times of these complexes are very similar (as it is common in exponential distributions), implying that an escape event resembles the dynamics of a particle trying to escape from a region through small passages [86].

By analyzing the motion of the complexes throughout the cell, it was found that the motion of the complexes that travelled from a pole to midcell is occluded. The regions where the anisotropies were higher were consistent with the location of the borders of

the nucleoids. Further analysis of cells with larger and smaller than average nucleoids, showed consistent spatial distributions of aggregates, suggesting that the spatial distribution of the complexes are defined by the size and location of the nucleoid in the cell.

To further prove that the nucleoid exclusion is responsible for segregating and retaining protein aggregates at the cell poles, it was studied the robustness of the segregation mechanism to changes in nucleoid size [7]. First, it was found that increasing and decreasing the nucleoid size causes an increase in the fraction of aggregates found in between the nucleoids prior to cell division. The reason for this aggregates' dynamic in cells with smaller nucleoids is the decrease in the interaction between aggregates and nucleoids, since the aggregates are less likely to locate near the nucleoids. Meanwhile, the reason for the increased fraction of aggregates in between larger nucleoids is reduced size of the polar regions, causing increased molecular crowding that forces the aggregates to move to the midcell. In conclusion, the segregation of protein aggregates is a process driven by the nucleoid-exclusion phenomenon.

3.1.3 Polarization of Tsr clusters

Tsr is one of the most abundant chemoreceptors [73], making it a prime substance to study the chemotaxis network. In normal conditions, approximately 7 % of Tsr proteins diffuse in the cell at all times [87]. Several studies have focused on how the chemotaxis complexes migrates to the poles. While some results suggested that the chemoreceptor clusters attach to the cell membranes, being dragged to the poles when cell division occurs [88], other results instead suggested that the clusters diffuse in the cell and that the matching curvatures of the clusters and the cell poles is responsible for the clusters' tendency to locate at the poles [89] (depicted in Figure 3.3). Some recent studies also suggest that the clusters preference for the poles results from a diffusion-and-capture mechanism [90] (depicted in Figure 3.3). In this mechanism, a chemoreceptor diffuses through the cell until a target protein at the cell pole captures it [91]. In this regard, a study proposes that a target protein that is responsible for the capture of chemoreceptor clusters is Tol-Pal [92], a protein complex inserted the *E. coli*'s envelope [93].

However, these studies also observed that the chemoreceptor clusters diffusion space is, to some extent, restricted to the same pole through consecutive generations [88]. They have also observed that the disruption of the cytoskeletal protein MreB (causing the cells to become round) leads to fragmentation of the Tsr patches at the poles and, consequently, an increase in the fraction of mobile Tsr [87]. These findings suggest that there is another mechanism, besides diffusion-and-capture by Tol-Pal complexes,

that is also responsible for the polarization of the chemotaxis network and that is disrupted when the cell shape is disrupted.

To address this, one study used Tsr labeled with fluorescent Venus proteins — with a similar mobility to unlabeled Tsr [87] — to investigate if the nucleoid-exclusion contributes for the polar preference of the chemoreceptor clusters and, if so, to which extent [6]. It was observed that the spatial distribution of Tsr-Venus is consistent with a nucleoid-exclusion phenomenon. One evidence for this is that the spatial distribution of Tsr-Venus was affected by asymmetries in the nucleoid position or changes in its length. To further examine the impact that the nucleoid has in the location of Tsr clusters, it was used cells lacking Tol-Pal complexes and cells lacking nucleoids. It was found that, in the absence of Tol-Pal complexes in the cells, the fraction of Tsr cluster at the poles decreases, even though it still higher than it would be if the clusters were uniformly distributed in the cell. In addition, in cells where the nucleoid is absent, the fraction Tsr clusters at the poles decreases as well. This provides evidence that the nucleoid exclusion contributes to the polarization of the chemotaxis network (as depicted in Figure 3.3) and that this phenomenon and the diffusion-and-capture mechanism by Tol-Pal complexes have complementary effects. In conclusion, the chemotaxis network depends on the length and position of the nucleoid.

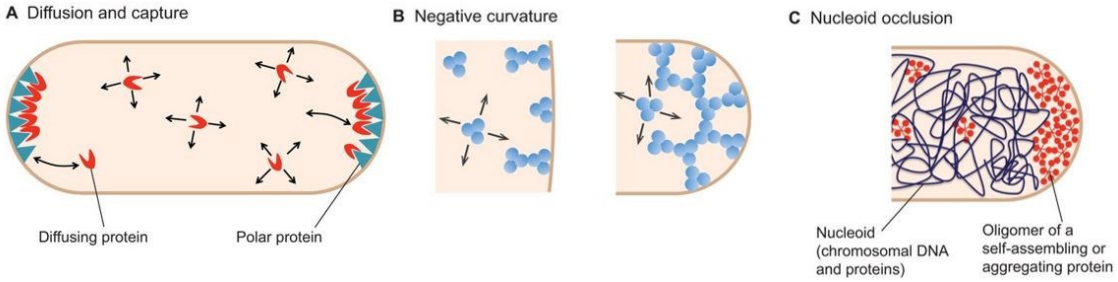

Figure 3.3. *Possible mechanisms responsible for the polarization of the chemotaxis network in E. coli. (A) The diffusion-and-capture mechanism, where a polar protein captures a diffusing receptor cluster, bounding it to the polar region. (B) The negative curvature effect, where matching curvatures (represented here as the variable C) between the cell poles and the chemoreceptor patches favors location of the clusters at the cell poles (blue regions) rather than at midcell (gray region). (C) Nucleoid exclusion phenomenon, where the high density of the nucleoid occludes the central region of the cell and "pushes" the chemoreceptor clusters to the poles. Image adapted from [91].*

3.2 Partitioning of cellular components

Assuming as a goal the perfectly symmetric partitioning of cellular components in cell division, the errors in partitioning, Q_x^2, can be quantified by the difference between the number of molecules inherited by each daughter cell [3]:

$$Q_x^2 = \frac{\left\langle (N_L - N_R)^2 \right\rangle}{\left\langle x \right\rangle^2} \tag{3.1}$$

where $\langle X \rangle$ is the mean value of X of each cell of the population, x is the number of molecules that exist before division and N_L and N_R are the numbers of molecules that were inherited by the left and right daughter cell, respectively. For molecules that exist in abundance ($\langle x \rangle$ >> 1), Q_x^2 will be very low. If, however, for other, less copious, molecules, small differences in partitioning cause significant errors in partitioning.

If there are segregation mechanisms responsible for the molecule's spatial distribution, they can be categorized as disordered — if they increase Q_x^2 — or ordered — if they decrease Q_x^2. Disordered and ordered segregation processes are depicted in Figure 3.4 (A) and (B), respectively.

In a disordered segregation process, if the cell divides in a random position, the daughter cells will have different sizes and, as a result, accommodate different amounts of various cellular components. If a cellular component spatial distribution is dependent of another, larger, component, then the volume available for the former component is restricted, causing it to be restrained to particular regions and, thus, partition in different numbers between daughter cells. Finally, if the cellular components are clustered and these clusters are divided between the daughter cells, there is a higher propensity for asymmetries between them.

In ordered segregation mechanisms, if the cellular components are large, their volume will make them exclude each other, causing them to distribute uniformly inside the cell. If the cellular components that diffuse without restrictions are bound to other, nonmoving, components, then their distribution in the cell can be such that their partitioning in cell division has a lower variance between daughter cells. Lastly, if the cellular components form pairs that are then split into separate daughter cells, then the partitioning between sister cells will be more symmetric.

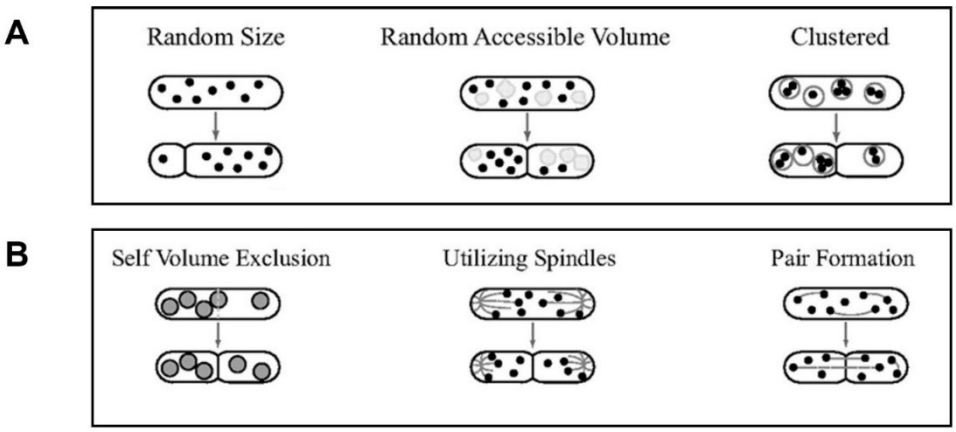

Figure 3.4. *Segregation processes. (A) Examples of disordered segregation processes: (left) cell division in a random position, (center) volume-exclusion phenomenon caused by larger cellular components, (right) components aggregate into cluster. (B) Examples of ordered segregation processes: (left) large components exclude each other and diffuse uniformly in the cell, (center) components bind to other stationary components, (right) components form pairs that are split between the daughter cells in the cell division process. Image adapted from [3].*

These segregation processes will generate different degrees of asymmetry in the partitioning of the cellular components between daughter cells. Among others, they lead to perfect partitioning (where individual components are equally divided between daughter cells), preferential partitioning (where individual components are partitioned according to a biased binomial distribution) or all-or-nothing partitioning (where all of the components are inherited by only one of daughter cells), which have increasing levels of asymmetry.

One study investigated how different partitioning schemes of nonfunctional proteins, could affect the growth rate of individual cells of a generation [94]. It was found that increasing asymmetry in partitioning schemes increases the population mean division time. Interestingly, apart from the all-or-nothing partitioning (which is unlikely to occur in natural biological systems), the cluster formation is the best partitioning scheme, as it reduces the mean division time of the population. Finally, it was also found that the bias of the preferential partitioning schemes of nonfunctional proteins increases with the increase of polar retention strength.

3.3 Diffusion of cellular components in the cytoplasm

One study [95] found that the bacterial cytoplasm behaves like a liquid for small cellular components, but it behaves like a glass-forming liquid that is approaching glass transition for larger cellular components. This dual behavior might arise from the high molec-

ular concentration that overcrowds the cytoplasm, as estimations indicate that macromolecules occupy 20 % to 40 % of the cytoplasm, with an additional 20 % of the cytoplasm (approximately) being occupied by water acting as a hydration layer to macromolecules. Overall, the excluded volume of the cytoplasm is expected to range from 40 % to 60 %.

Furthermore, the cell's metabolic activity "fluidizes" the cytoplasm by suppressing its glass-like properties and this effect is increasingly notable for increasingly larger molecules. To understand the reason for this effect, it must be considered that the macromolecules in the cytoplasm, by electrostatic and hydrophobic interactions, create extremely crowded regions separated by less crowded areas named nanopools [96], as depicted in Figure 3.5. When metabolic activities disrupt the hydrophobicity and charge of the molecules, causing them to rearrangement, the configuration of nanopools change. Thus, any molecule that was previously inside a nanopool (associated to glassy dynamics) becomes able to diffuse again (associated to liquid dynamics).

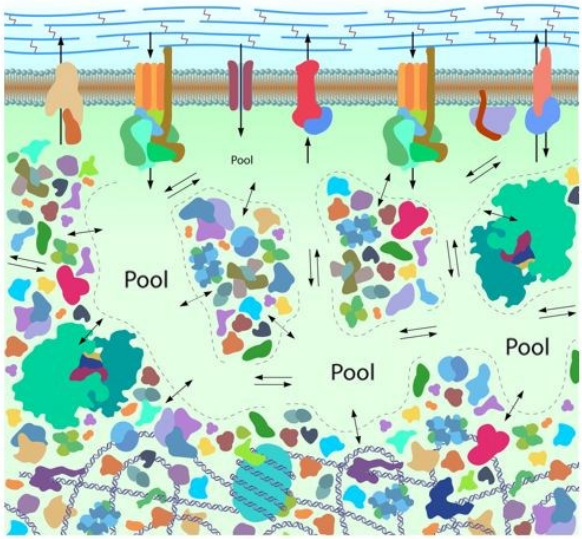

Figure 3.5. *Cytoplasmic overcrowded regions separated by nanopools. Image adapted from [97].*

This cytoplasmicity has consequences, such as different diffusion rate constants for different-sized molecules. Cellular components such as proteins will navigate in the cytoplasm as if it was a liquid, while components larger than 300 nm (such as plasmids, protein filaments and polyribosomes) will have a metabolism-dependent diffusion pattern. However, the fluidization caused by metabolic activity can be useful to achieve a high concentration of macromolecules without significantly hampering their movement inside the cell.

3.4 Effects of temperature shifts on *E. coli* cells

The temperature a cell is subjected to will affect its properties and processes. Several studies have been conducted to understand the consequences of nonoptimal temperatures, and how cells react to temperature shifts. One study [98] found that the mean cell volume remains constant from 15 °C to 30 °C, varying slightly toward smaller volumes at 40 °C and toward larger volumes and 11 °C. Temperature shifts, however, cause temporary increases (when the temperature decreased) and decreases (when the temperature increased) in cell volume.

Another study [99] investigated how the temperature affects the protein synthesis processes. Since the rate of protein accumulation is determined by the number of working ribosomes, the rate they are working at, and the rate of protein degradation, this study observed how these three parameters changed with temperature. It was found that the number of ribosomes remains constant between 25 °C and 37 °C. It was also found that the peptide elongation rate increases with temperature, even when the temperature increases from the optimal temperature of 37 °C to 44 °C, demonstrating that the working rate of the ribosomes is not a limiting factor for cell growth at high temperatures. However, it was observed that, at 15 °C, there is an increase in the amount of non-translation ribosomes, suggesting that there are difficulties in transcription initiation at lower temperatures. Finally, the study also showed that, at high temperature, the protein degradation rate increases drastically.

In order to understand the robustness of the protein aggregates segregation, one study observed how this mechanism responds to nonoptimal temperatures [100]. It was found an increase in the fraction of aggregates at midcell for temperatures lower than 37 °C, which changes in the nucleoid's size could not explain. Since the aggregates diffuse (even when retained at the poles [23]), it was hypothesized that the reason for the decreased effects of the nucleoid-exclusion phenomenon was changes in the cytoplasm viscosity. Therefore, the relative dynamic viscosity was measured in different temperatures and it was found that it increases as temperature decreases, suggesting that the variations in the aggregates spatial distributions are due to changes in the thermophysical properties in the cytoplasm. This can have repercussions in the cell's survival, as low temperatures can cause the aggregates to segregate less to the poles and, likely, decrease the mean population growth rate.

4. RESEARCH METHODOLOGY AND MATERIALS

The data in this project results from analysis of the results of the experiments carried out in [6], [8] and [100]. In this chapter, we delve the main techniques used to collect and analyze the empirical data. It begins with an introduction to the laboratorial procedures, such as microscopy, followed by a description of the software tools used to process images and a brief description of the methods used analyze the data.

4.1 Strains

An organism as *E. coli* can have multiple variations in its genome, creating different strains. In order to study different aspects of the cell, several strains have been engineered, to better test the hypotheses. In this thesis, different strains were used to study the various cellular processes.

To track the spatial distributions of protein aggregates, it was used the strain DH5α-PRO to which were added two genetic constructs to produce the fluorescent MS2-GFP-RNA (further explained in section 4.2.2) and the plasmid pAB332 carrying *hupA-mcherry* (controlled by the constitutive promoter, hupA) to ensure the validity of the DAPI measurements on the nucleoid's size and position. [100]

To assess how the symmetry in the placement of the Z-ring changes with changes in temperature, it was used the BS001 strain (derived from the strain MG1655), which expressed FtsZ-GFP under the regulation of P_{lac} [8]. The strain MG1655 was also used to visualize the positioning of Tsr clusters. Particularly, it was used an isogenic derivative strain MG1655, termed Δ*tolpal*, in which Tol-Pal was absent and with a pBR322-derivated plasmid, coding for the *tsr-venus* gene, under the control of the P_{lac} promoter [6].

4.2 Methods for detecting the location of cellular components

In this thesis, to study the spatial distribution and dynamics of cellular components, we make use of fluorescent probing. In this phenomenon, when the molecule absorbs a photon, it goes from its ground state to an excited one [101]. One way to return to its

ground state is through fluorescence. In this process (illustrated in Figure 4.1), the excited molecule loses vibrational energy (non-radiative) through collisions with other molecules, until it reaches the lower vibrational level in the excited electronic state [101]. Then, when the molecule returns to its fundamental state, it releases a photon of lower frequency (higher wavelength) from the one it received [101]. This photon is what causes the molecule to become luminescent. This phenomenon can be used to detect components in a cell by using microscopy techniques where the photon of higher wavelength is filtered out, leaving only the emitted light.

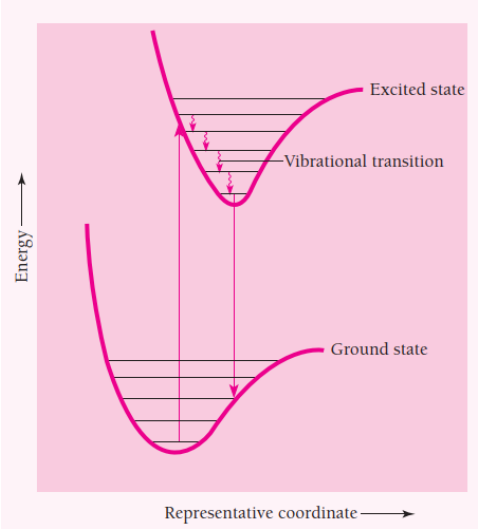

Figure 4.1. *Scheme of the molecular states in the fluorescence process. When the molecule absorbs radiation, it goes from a ground state to an excited state. Then, by collisions with other molecules, it loses energy through vibrational transitions. When it reaches the lower vibrational level in the excited state, it releases a photon when transitions to the ground state. This photon emits radiation in the and makes the molecule fluorescent. Image adapted from [101].*

For the past decades, the use of fluorescent molecules has been the dominant technique in cell biology studies using microscopy. The recent development of a wide variety of fluorescent proteins has allowed the visualization of specific structures in live cells with a better spatial resolution that fluorescent dyes. In this section, we explore some of these fluorescent techniques, namely DAPI staining and tagging by fluorescent proteins.

4.2.1 Nucleoid imaging by DAPI staining

The morphology of the nucleoid of *E. coli* is sensitive to growth rate, richness of growth medium and application of external perturbations [9]. Using the combination of DNA dyes along with electron microscopy has allowed researchers to detect these changes in morphology. To better visualize the nucleoid, a fluorescent stain should permeate

the cell membranes, bind to the DNA and emit strong and long-lasting luminescence. Further, it should not affect the cell's functioning nor the nucleoid's morphology.

One of most popular fluorescent stains for nucleoid is the DAPI (4', 6-diamidino-2-phenylindole) stain [148]. This DNA-specific stain permeates the cell membranes and associates to A-T regions, binding to the minor groove of DNA in both live and fixed cells, as depicted in Figure 4.2 (A) [102]. The DAPI stain can be observed using epifluorescence microscopy with a mercury lamp and a DAPI filter. The dye is excited at ~350 nm and emits at ~450 nm (example image in Figure 4.2 (B)).

This stain has some limitations, such as the high concentrations needed for the proper imaging of live cells, which can be toxic to the cells. Moreover, the use of UV lights and the fact that the DAPI is an intercalating dye can affect the apparent morphology of the nucleoids by expanding it.

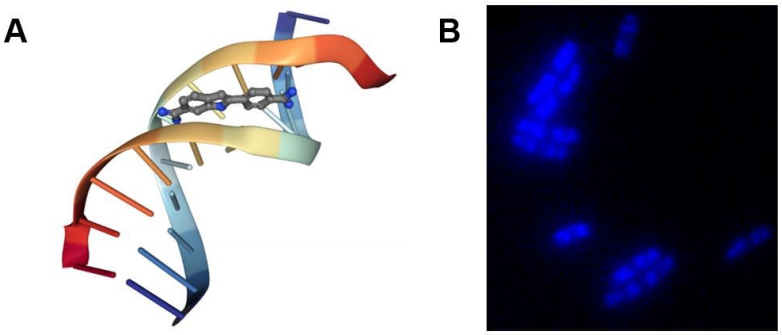

Figure 4.2. *DAPI stain. (A) Scheme of DAPI binding to the DNA. (B) DAPI-stained cells observed using epifluorescence microscopy. Image (A) taken from [103] and image (B) adapted from [104].*

4.2.2 Fluorescent protein tagging

In 1961, while studying the illuminating jellyfish *Aequorea*, Shimomura and colleagues found the luminescent substance aequorin, which generated a bright blue light in the presence of calcium [105]. During its purification, they found the green fluorescent protein (GFP). Eventually, techniques were developed that allowed GFP to be used as a fluorescent marker, *in vivo*, of molecular components within cells [106]. Since then, several other fluorescent proteins (FPs) have been developed, each with specific spectral properties, sensitivity and photostability, making them suitable to study a wide range of processes and conditions and, thus, ubiquitous in the biological imaging field [107]. Due to this, FPs have been used to visualize cellular structures (with an increased spatial resolution when compared with dyes) and their dynamics, which has

contributed to a better understand the various processes that are at the single-cell, single-molecule level [108], [109].

Compared to staining molecules like DAPI, the concentration of fluorescent proteins necessary for detection is usually not toxic for the cells. Also, fluorescent proteins do not need cofactors (apart from oxygen, necessary for the generation of the chromophore) [110]. However, they also have some limiting factors regarding brightness and photostability. Therefore, one must take all these properties and drawbacks into consideration when choosing a FP tagging system to ensure its detection — the emitted fluorescent signal needs to be higher than the background fluorescence (autofluorescence) — and to guarantee that the natural functioning of the components that are tagged with the FP is not disturbed.

FPs offer an alternative form to observe the nucleoid, through the fusion of fluorescent proteins, such as mCherry, to nucleoid associated proteins (NAPs). Namely, the protein Huα, a subunit of the HU protein (which aids in DNA compaction), has been found to accurately inform on the spatial distribution of the nucleoid [9]. The *hupA* gene, which codes Huα, fused with the *mCherry* gene can either be inserted in the chromosome or maintained on a plasmid that is then transferred into the host [9]. Using fluorescent microscopy, the nucleoids labeled with HupA-mCherry become visible, as seen in Figure 4.3.

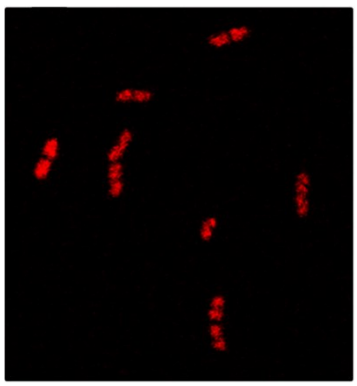

***Figure 4.3**. Example image of HupA-mCherry labelled nucleoids using confocal microscopy. Image adapted from [104].*

The GFP tagging method is used to visualize molecules inside the cell and it can be used in a variety of ways. For example, the MS2-GFP system (Figure 4.4 (A)) is used to track individual RNAs *in vivo* [111]. This method requires two genetic constructs: a construct that codes for the target gene fused with a tandem array of MS2 binding sites (the binding sites adopt a stem-loop structure after being transcribed) and a construct that codes for the MS2 coat protein (which binds to the 21nt genomic RNA [112]) fused to the GFPmut3 (a variation of GFP). These constructs can be engineered into a plas-

mid or integrated into the cell's chromosome. In the cells used in this project, the MS2-GFP proteins are produced by a medium-copy vector and the target RNA is produced by a single-copy F-plasmid. Figure 4.4 (B) shows how the target RNA (with several MS2-GFP bound to it) appears as a bright spot inside the cell when using confocal microscopy. This allows analyzing the RNA's position and track transcription events [113]. The MS2-GFP method offers advantages such as the non-degradation of the RNA coated by MS2-GFP proteins (lifetime longer than 2 hours) [113] and the complex's resistance to photobleaching [114].

These two properties, along with its size, make the MS2-GFP-RNA complex a prime option to study the spatial kinetics of nonfunctional protein aggregates, informing on the *in vivo* spatial distribution of protein aggregates [100]. Nevertheless, it also has some drawbacks, namely the heterogeneous binding of MS2 might affect its quantification and the RNA's natural mobility. In this project, the GFP label was also used in FtsZ-GFP, whose expression is under the control of the P_{lac} promoter [115].

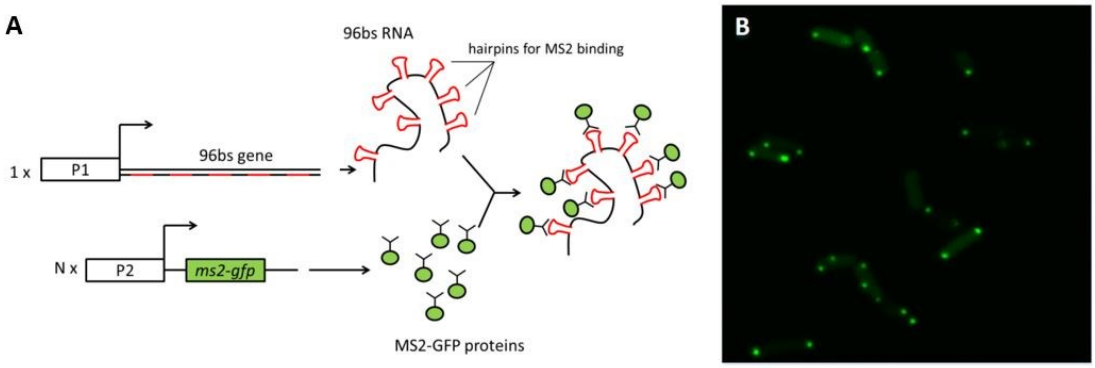

Figure 4.4. *MS2-GFP tagging method. (A) Scheme of formation of MS2-GFP-RNA complexes. The gene with the target RNA, controlled by a single copied promoter (P1) — in this thesis is $P_{lac/ara-1}$ — is fused with 96 binding sites (represented in red), creating an RNA with hairpin structures for MS2-GFP proteins. These proteins (represented as green circles with hooks) are formed in another construct in a multi-copy plasmid controlled by a promoter (P2) — in this thesis is $P_{LtetO-1}$. When an RNA from the target gene forms, the MS2-GFP proteins bind to its binding sites, creating a fluorescent spot. (B) Confocal microscopy image of E. coli cells expressing RNAs labelled with MS2-GFP proteins. Each RNA molecule appears as a fluorescent spot, while the background fluorescence in the cell is due to freely diffusing MS2-GFP complexes. Image (A) adapted from [34] and image (B) adapted from [104].*

To study the production of proteins molecules in *E. coli*, Yu and colleagues develop the Tsr-Venus system [116]. As depicted in Figure 4.5 (A), the genetic construct that originates the Tsr-Venus complex was inserted in the host chromosome and is formed by the fusion of the *venus* gene (that originates the Venus protein, a variant of YFP) with the *tsr* gene (that originates a Tsr chemoreceptor), under the control of the *lac* promot-

er. Since Tsr chemoreceptors are abundant in the cell, the small amount of Tsr-Venus produced by this non-native genetic construct does not affect significantly the cell's functioning. The Venus fluorescent protein makes the Tsr-Venus cluster visible using confocal microscopy, as seen in Figure 4.5 (B), allowing this system to study the spatial distribution of the chemotaxis network.

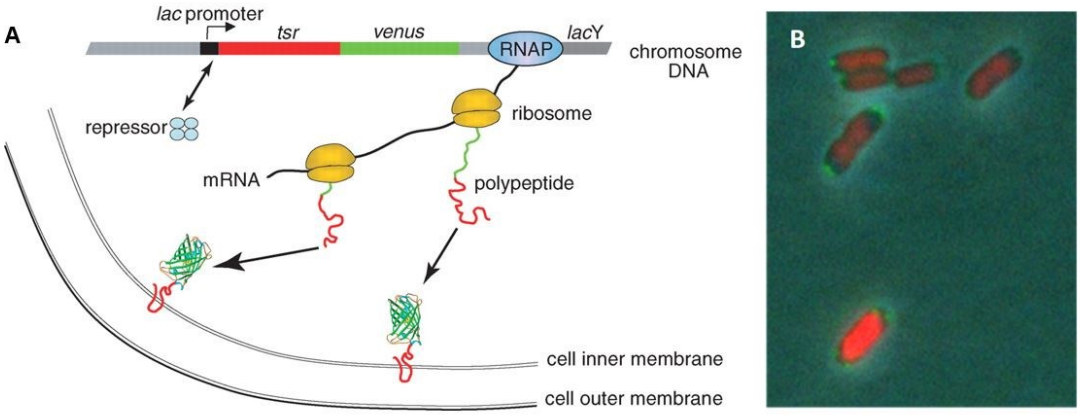

Figure 4.5. *Tsr-Venus label system. (A) Diagram of the formation of Tsr-Venus clusters. The genetic construct of the tsr gene fused with DNA that code the fluorescent Venus protein. When transcribed and translated, the Tsr protein, connected to the N-terminus of the Venus protein, migrates to the cell membrane where the complex remains, visible as a fluorescent spot. (B) Merged fluorescent microscopy images of Tsr-Venus clusters (green), nucleoids labelled with HupA-mCherry (red), overlaid with the phase contract image. Image (A) adapted from [116] and image (B) adapted from [104].*

Though fluorescent proteins provide a solution to study cellular components, they have some drawbacks. Limitations in photostability [117] and long maturation times (the time it takes for a FP to undergo various steps until it becomes fluorescent), — which are not short enough to detect the labelled components as soon as they are produced — decrease the FPs usability. There can also be fluctuations in the brightness of the FP (blinking phenomenon), photobleaching (when an FP interacts with other molecules and loses its fluorescent capability) and alterations of the tagged components functioning [118], which hampers the image.

4.3 Microscopy

The molecular biologists of the Laboratory of Biosystem Dynamics obtained the microscopy images used in this thesis. This section covers the microscopy techniques that were used to obtain such images, namely fluorescent microscopy, phase-contrast microscopy. It is also described how a temperature regulator was used to place cells at different temperatures while under observation.

4.3.1 Fluorescence Microscopy

Many fluorescence microscopy methods allow the visualization of cellular components in bacterial cells. The most commonly used is the epifluorescence microscopy (also known as wide-field epifluorescence), where an area of approximately $10 \times 10\ \mu m^2$ [119] is illuminated. As the volume illuminated is quite large, this method has the ability to perform faster imaging; nevertheless, this larger volume can also cause out-of-focus fluorescent signals, which increases the background fluorescence and lower spatial resolution [120]. Then, this method is normally used with strong fluorophores as probe molecules [119].

There are microscopy techniques that suppress background fluorescence more efficiently by reducing the out-of-focus light through the reducing of the fluorescent signal from the sample that the detector captures. One of these techniques is confocal microscopy, which reduces the focal volume of the sample that is illuminated to less than $1\ \mu m^3$ [119]. It does this through a pinhole aperture that ensures that any light that is not from the plane where the excitation light was focused on (that is, light that is not from the confocal plane) does not reach the detector, as depicted in Figure 4.6 [120]. The volume illuminated in the sample is reduced in confocal microscopy, resulting in better spatial resolution but also a decrease in the speed of the imaging process, which can be critical when studying cellular mechanism with fast dynamics. However, there are some variations of the technique that increase the speed of imaging such as spinning-disc confocal microscopy, which uses a disc with several pinholes or slits (instead of a single pinhole), causing several regions of the sample to be illuminated simultaneously (also decreasing phototoxicity) [121].

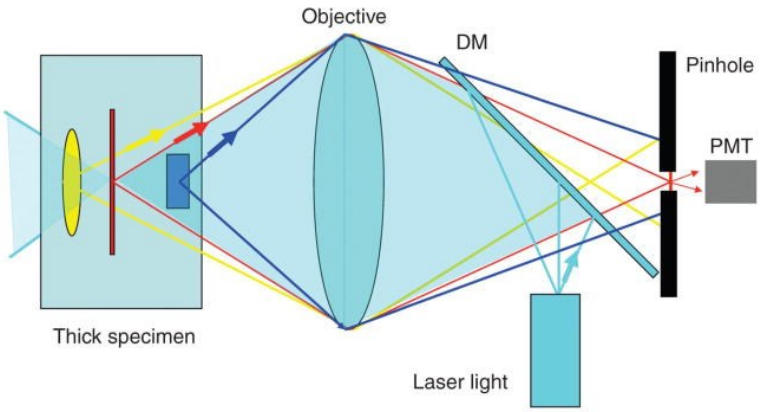

Figure 4.6. *Diagram of functioning of confocal microscopy. The laser light (represented here as light blue beams and shade) is reflected on the dichroic mirror (DM), passes the objective lens and hits the thick specimen. This light excites the fluorescent molecules, and their luminous signal they emit passes through the objective lens and the DM, reaching the image plane (represented here has colourful yellow, red and blue beams). However, the pinhole aperture only allows the signal from the confocal plane (here represented as red beams) to pass and reach the photomultiplier tube (PMT, the detector). Image adapted from [120].*

The microscopy images used to visualize the DAPI stained nucleoids were obtained through epifluorescence microscopy. The microscopy images of fluorescent spots of complexes such as FtsZ-GFP, MS2-GFP-RNA and Tsr-Venus were obtained using confocal microscopy. Finally, cell segmentation was made using phase-contrast microscopy images, which will be discussed in section 4.3.2.

4.3.2 Phase-contrast microscopy

Developed by Zernicke in 1942 [122], phase-contrast microscopy allows the visualization of high-contrast images of transparent organisms without coloring them. Its working principle is the phase shift that the incident light suffers when passing through a sample (in this case, the phase shift that the light experiences when passing through a cell is nearly - 90 °) [123]. This occurs due to a decrease in the incident light speed inside the cell. Thus, the image plane results from the interference of the diffracted light (that passed through the cell) with the direct light from the illumination source (that did not go through the cell and, therefore, did not suffer a phase shift). Zernicke then created a phase plate (positioned between the objective and the image plane, as depicted in Figure 4.7 (A)) that lets the diffracted light pass to the image plane but shifts the direct light by 90 ° [123]. In the phase-contrast microscopy, images used in this thesis make use of negative phase contrast, in which the direct light is shifted by + 90 °. Then, the destructive interference between the direct and diffracted light beams cross, causing the cell to be darker than the background (Figure 4.7 (B)).

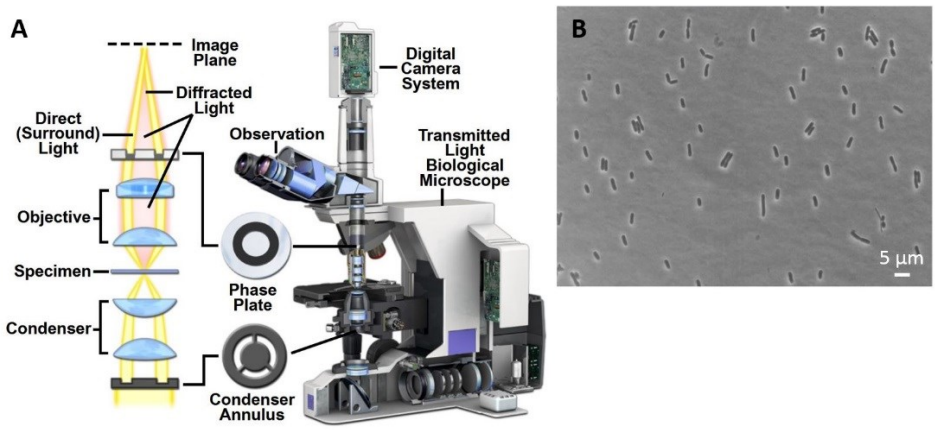

Figure 4.7. *Phase-contrast microscopy. (A) Scheme of functioning of phase-contrast microscopy. When the incident light (yellow beams) passes through a cell (in the specimen region), its speed decreases, creating a diffracted light (red shadow) with a phase shift. In contrast-phase microscopy, a phase plate in positioned before both types of light (direct light and diffracted light) reach the image plate. This plate creates a phase shift of 90 ° in the direct light, creating regions of constructive and destructive interference between both types of light that reveal the cells' shape. (B) Example of a phase-contrast image of E. coli cells. Image (A) adapted from [124] and image (B) adapted from [6].*

4.3.3 Temperature regulator

To study the consequences of temperature shifts in cellular processes, the cells must be visualized at different temperatures while in the microscope. For that it was used a thermo-chiller chamber, shown in Figure 4.8 (A)(C), with a thermo-chiller device that can impose temperatures ranging from 5 °C to 50 °C with a ± 0.2 °C uncertainty and microfluidic platform, depicted in Figure 4.8 (D), to ensure the continuous flow of fresh media during the imaging process [125].

In this device (placed on the stage of an inverted microscope, as depicted in Figure 4.8 (B)), the thermo-chiller device (connected to the thermo-chilled chamber) controls the temperature of the cells, while the micro-perfusion device (connected to the thermo-chilled chamber) provides a flow of fresh media and chemicals to the cells.

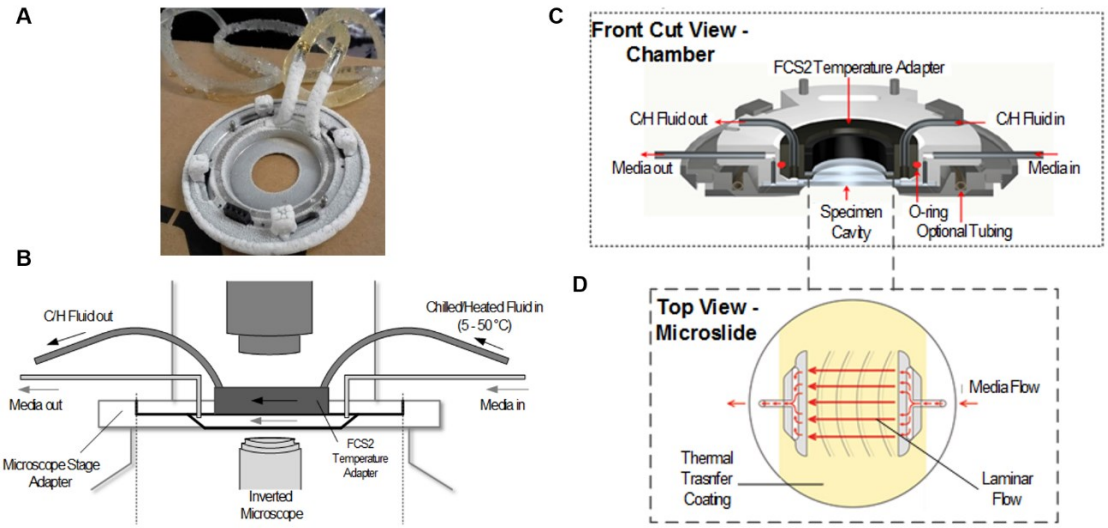

***Figure 4.8**. Temperature regulator. (A) Photo of the thermo-chiller chamber. (B) Scheme of placement and functioning of the temperature regulator. The inlet and outlet of a chilled/heated fluid regulates the temperature the cells are subject to. The cells are placed in a micro-aqueduct slide below the temperature adapter. An inlet and outlet of media ensures a continuous laminar flow of fresh media to the cells. The chamber is placed on the stage of an inverted microscope. (C) Front view schematic of the thermo-chiller chamber. (D) Diagram of the top view of micro-aqueduct slide, positioned inside the optical cavity. Image (A) adapted from [126] and images (B), (C) and (D) adapted from [125].*

4.4 Image processing and data analysis

Image processing tools, such as SCIP [127], were used to analyze the microscopy images, namely, to perform cell and nucleoid segmentation and fluorescent spots detection. These tools are needed to ensure an accurate and unbiased extraction of the cell's features. This section provides an overview of the computational tools and methods within used in this project for this analysis.

4.4.1 Cell and nucleoid segmentation

To detect and segment the cells in the microscopy images obtained it was an used a method similar to the software "CellAging" [128]. This method uses Gradient Path Labelling (GPL) algorithm [129]. This algorithm begins by labeling the pixels based on their azimuth. Then, the labels are propagated according to its gradient paths. Finally, classifiers are used to merge and discard the segments created. The resulting segmentation can then be corrected manually, creating segmentations as depicted in Figure 4.9.

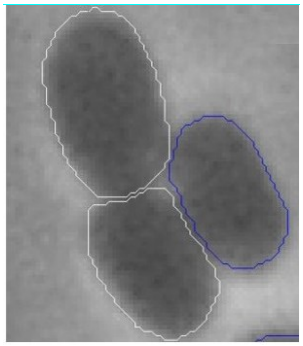

Figure 4.9. *Example of cell segmentation. The blue lines match the automatic segmentation and the white lines correspond to manual corrections. Image adapted from [127].*

For nucleoid segmentation it was also used the Gradient Path Labelling (GPL) algorithm [129]. Then, the number of layers was reduced by tagging labels as equivalents when they belong to the same maximum. Finally, the segmented image, such as the one in Figure 4.10, is created with the number of labels equaling the number of nucleoids.

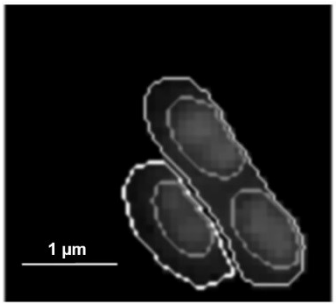

Figure 4.10. *Example of nucleoid segmentation with GPL (merged with the cell segmentation). The alignment of the phase-contrast images and the confocal images was made by a selection of 5 to 7 landmarks in both images and using thin-plane spline interpolation for the registration transform. Image adapted from [8].*

4.4.2 Fluorescent spots detection

To locate the border of the Z-ring, the FtsZ-GFP signal was detected from the background fluorescence using a threshold [130]. However, this algorithm was only applied to cells with a Z-ring in a closed ring state, making use of a machine learning algorithm that can distinguish the different phases of Z-ring formation from microscopy images, seen in Figure 4.11 [131]. Therefore, this classifier — using the Regularized Multinomial Logistic regression (RMLR) — can recognize the cells with a Z-ring in a closed ring state.

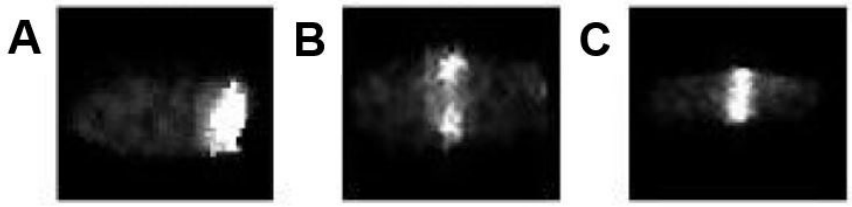

Figure 4.11. *Microscopy images of the different stages of the Z-ring formation. (A) FtsZ-GFP is positioned in one of the poles of the cell. (B) Open ring stage. (C) Closed ring state. Images adapted from [131].*

Spot detection for structures such as protein aggregates (depicted in Figure 4.12) and Tsr-Venus clusters, each fluorescent spot inside the cell was segmented using a kernel density estimation method [132]. This method measures the local smoothness in the image and identifies as fluorescent spots the areas with low smoothness. Then, the spot intensity is readjusted by subtracting the mean intensity of the cell's background multiplied by the area of the spot to the total fluorescence intensity of the spot [100].

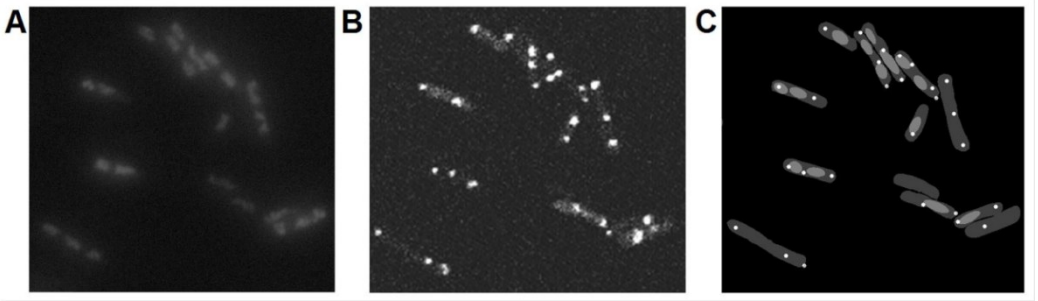

Figure 4.12. *Segmentation of fluorescent protein aggregates. (A) Cells with nucleoids stained with DAPI. (B) Cell with bright spots corresponding to RNA molecules tagged with MS2-GFP. The cells also have a visible cytoplasm with a low fluorescence level due to the diffusion of unbound MS2-GFP. (C) Merge of the segmented images of the nucleoids and the fluorescent spots. In the merging process, the resolution of the epifluorescence images was changed to the resolution of the confocal images by a 2D affine geometric transformation. Image adapted from [100].*

4.5 Linear correlations

In this project, we searched for linear correlations between variables using the least-squares regression fitting method. As depicted in Figure 4.14, in virtually every function fitting, most of the data points that are used to estimate the fitted curve are not inserted in it, but are distanced by an offset each. For linear fittings, the least-squares regression finds the values of a and b — that relate the variables x and y into the linear function $y = a \times x + b$ — which minimize the sum of the squares of the offsets of these data points.

We made use of the p-value as to assess the goodness of fit. The p-value represents the probability of a certain null hypothesis occurring. In this project, the null hypothesis is that y and x are uncorrelated (that is, the data points in the plot would be randomly scattered and best described by the function $y = b$). Then, after setting a significance level for which the null hypothesis is accepted (in this project is 0.1) and if the p-value is lower than such minimum acceptance value, the null hypothesis is rejected. In this thesis, the rejection of the null hypothesis of no correlation is interpret as the variables being linearly correlated.

4.6 Definition of efficiency and robustness

Biophysical factors such as the nucleoid(s) size and position, protein clusters' size (here MS2-GFP-RNA aggregates and Tsr-Venus chemotaxis clusters) are expected to affect cellular functioning.

Since *E. coli* cells exhibit high symmetry in division, we assume that each cell aims to place the Z-ring at the center of its major axis. Similarly, since protein aggregates and Tsr clusters are usually placed at the cell poles, we assume that the cell aims to place them at one of its extremities.

In order to quantify efficiency and robustness of these processes in a cell population, we first normalize the cells' length along the major axis to 1, with the center being at 0, as depicted in Figure 4.14. Given this, the position of any cellular component will be in a range of [- 0.5, 0.5]. We also assume (given the measurements reported in [6]) that the nucleoid occupies the interval [- 0.25, 0.25].

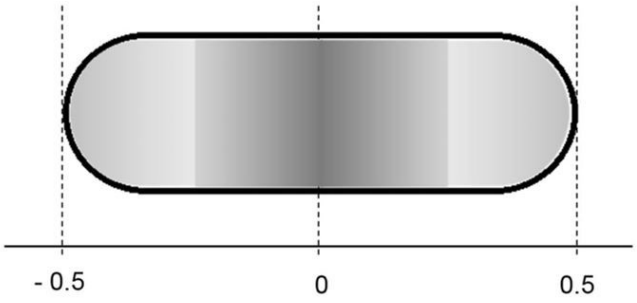

Figure 4.13. *Normalization of the length of the E. coli cell's major axis. The center of the cell is the position 0 and the cell extremes are positioned at - 0.5 and 0.5. The midcell region is in darker grey and the polar regions are represented by a lighter gray.*

Given all of the above, Efficiency (E) is here quantified making use of measurements of the distance that a given component is from its ideal position. Let D be the distance of the component from the cell center and E_Z^i, E_A^i and E_{Tsr}^i be the efficiency in placing

the Z-ring, a protein aggregate and a Tsr cluster in their ideal positions, respectively. We assume this ideal position to be midcell for the Z-ring and to be cell polar extremity for protein aggregates and Tsr clusters.

If $\langle X \rangle$ and $|X|$ are the average and the absolute value of a variable X, respectively, and n is the number of components j in the cell, then the efficiencies of the processes of placement of the Z-ring, protein aggregates and Tsr clusters can be quantified by:

$$0 \le E_Z^i = \frac{1}{2} - |D| \le \frac{1}{2} \tag{4.1}$$

$$0 \le E_A^i = \sum_{j=1}^{n} \frac{\langle |D_j| \rangle}{n} \le \frac{1}{2} \tag{4.2}$$

$$0 \le E_{Tsr}^i = \sum_{j=1}^{n} \frac{\langle |D_j| \rangle}{n} \le \frac{1}{2} \tag{4.3}$$

Therefore, a process in which all the components in a cell are placed in the 'ideal' position will have an efficiency of 0.5. When all components are maximally displaced from their ideal position the efficiency is 0. We used these equations to quantify how effective is the placement process of the three cellular components in a certain condition.

Changes in the environmental conditions, such as temperature shifts, are expected to change the aforementioned biophysical factors, which, in turn, may perturb the placement of the cellular components, affecting the efficiency in this positioning.

We thus quantified the robustness of these processes to environmental shifts making use of quantitative comparisons between their efficiencies in a given condition relative to the efficiency in optimal conditions. Let n_c be the number of nonoptimal conditions tested. We define the robustness R of the cell population to be:

$$R = \frac{1}{n_c} \cdot \sum_{j=1}^{n_c} \frac{E_j}{E_{control}} \tag{4.4}$$

If the efficiency of a process is lower in nonoptimal conditions than in the optimal condition, R will be lower than 1. Else, it will be larger than 1 (which is unlikely to occur).

5. RESULTS AND DISCUSSION

In this chapter, we present the results of the project. In the previous sections, it was described how the nucleoid(s) — either a single nucleoid in the cell or two nucleoids when chromosome has replicated but the cell has not yet divided — act as a source of spatial organizer of cellular components, such as the Z-ring, nonfunctional protein aggregates and chemotaxis protein complexes. Thus, to study the extent to which the nucleoid exclusion phenomenon plays a part in the placement of the Z-ring, in the segregation of protein aggregates and in the polarization of chemotaxis cluster (such as the Tsr clusters studied in this project), we determined the efficiency of these processes. We also determined how this efficiency shifts with changes in temperature, that is, so as to investigate their robustness to nonoptimal conditions.

5.1 Influence of temperature in nucleoid morphology

Using the microscopy images from [141], the morphology of the nucleoids, here assessed by measuring the size and position of DAPI-stained nucleoids, was measured for four temperature conditions (10 °C, 24 °C, 37 °C and 43 °C). Since the width of the nucleoid (length along the minor cell axis) did not change significantly with varying temperatures, the nucleoid's size shown here is its length (that is, the length along the major cell axis). For cells with two nucleoids, this length includes the two nucleoids and the distance between them. The results are shown in Figure 5.1.

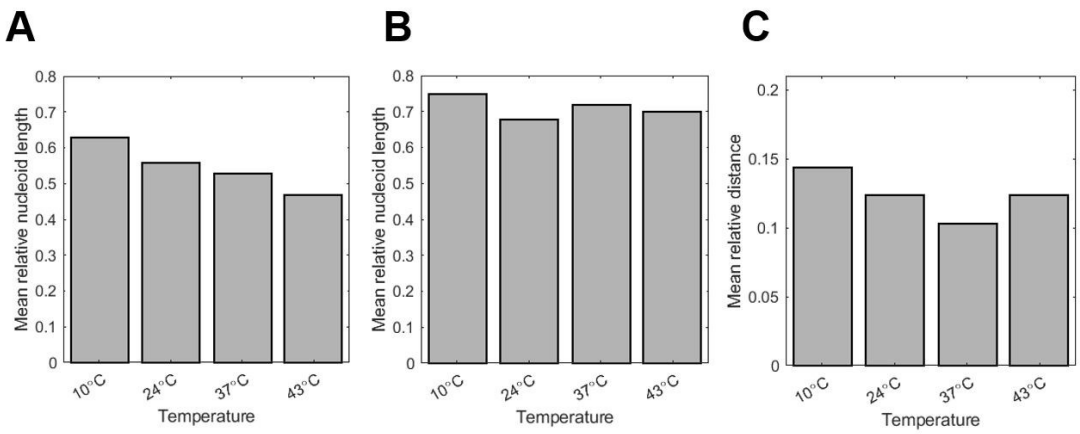

Figure 5.1. *Nucleoid length along the major axis at different temperatures.(A) Mean nucleoid length for cells with one nucleoid at 10 °C, 24 °C, 37 °C and 43 °C. (B) Mean length of the nucleoids (and space in between) for cells with two nucleoids at 10 °C, 24 °C, 37 °C and 43 °C. (C) Mean distance between the nucleoids (distance between the borders of the nucleoids closest to the cell center) at 10 °C, 24 °C, 37 °C and 43 °C.*

From Figure 5.1, the nucleoid(s) morphology changes with temperature. From Figure 5.1 (A), the nucleoid size decreases with increasing temperature (in accordance with [100]), with a difference of approximately 15 % between 10 °C and 43 °C. Also, from Figure 5.1 (C), the distance between the nucleoids is minimal at 37 °C (in agreement with [10]), with a shift of approximately 5 % between 10 °C and 43 °C. The combination of the changes in size and in distance result in the changes in relative length of the two nucleoids shown in Figure 5.1 (B). Overall, we expect that the spatial distributions of the Z-rings, protein aggregates and Tsr clusters will change with temperature.

5.2 Spatial distribution of cellular components

Having confirmed that the temperature affects the nucleoid(s) morphology, we obtained the distribution of the cellular components' absolute distances along each cell's major axis (relative to the cells' length) from their optimal position. Figure 5.2 shows the single-cell distribution of the distance between the Z-ring and the cell's center. Figure 5.3 shows the single-cell distribution of the distances between the MS2-GFP-RNAs (protein aggregates) and the cell poles (closest pole). Finally, Figure 5.4 shows the single-cell distribution of the distances between the Tsr clusters and the (closest) cell pole.

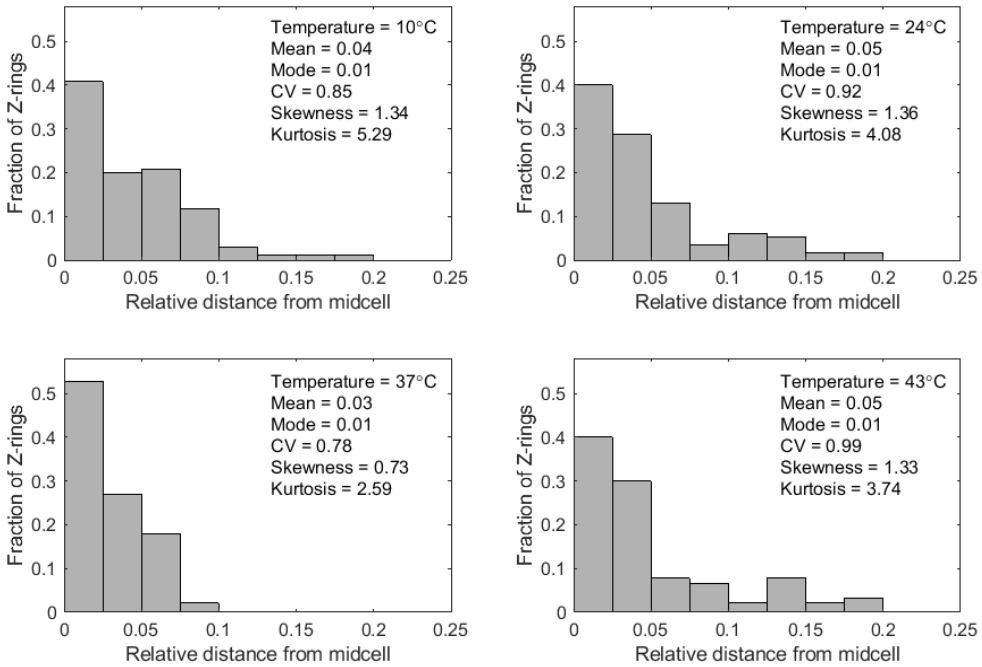

Figure 5.2. *Distribution of distances (relative to the cell length) between the Z-ring and midcell at 10 °C, 24 °C, 37 °C and 43 °C and for more than 100 cells in each temperature. Each graph has an inset informing on the temperature and the distribution, namely the mean, mode, coefficient of variation (CV), skewness and kurtosis. Note that the few Z-rings that were distanced more than 0.2 from midcell were excluded as, in those cases, the Z-ring was observed to have formed outside the space between the nucleoids (see Figure 5.5 (C)), which results in at least one nonfunctional daughter cell (without a nucleoid).*

From Figure 5.2, at all temperatures considered, the spatial distribution of Z-rings behaves in conformity with the distances between nucleoids (Figure 5.1 (C)). From 10 °C to 37 °C, it is visible a gradual decrease in the distances from midcell, minimizing at 37 °C and increasing again at 43 °C. This supports the hypothesis that the distance between the nucleoids affects the uncertainty of Z-ring's distance from midcell.

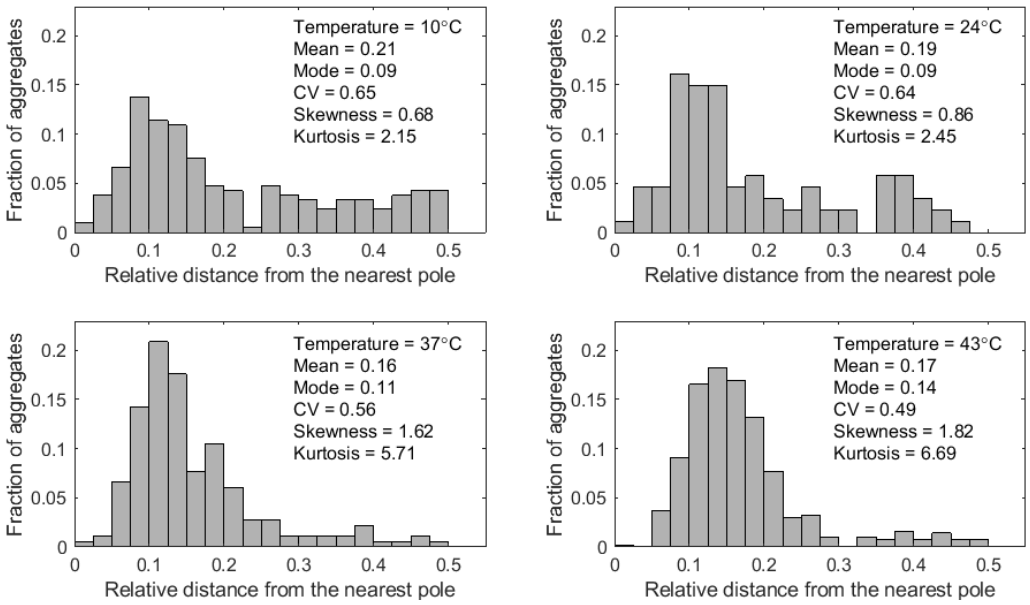

Figure 5.3. *Distribution of distances (relative to the cell length) between the MS2-GFP-RNA complexes' position and their nearest cell pole for 10 °C, 24 °C, 37 °C and 43 °C and for more than 100 cells in each temperature. Each graph has an inset with the temperature and information about the distributions, namely their mean, mode, coefficient of variation (CV), skewness and kurtosis.*

Figure 5.3 informs on the distribution of distances of single-aggregates (MS2-GFP-RNA complexes) from the closest cell pole at the various temperatures. Visibly, the mean of the distribution is minimal at 37 °C. The decrease in the distance from the nearest cell pole seen from 10 °C to 37 °C is likely due to the increase in cytoplasmic viscosity with decreases in temperature [141], making it harder for macromolecules, such as protein aggregates, to diffuse inside the cell (in this case, to migrate to the poles). Meanwhile, the increase in 43 °C is likely due to the decreased length of the nucleoid, with increasing temperature (Figure 5.1 (A)). Overall, the results suggest that, at 37 °C, there is an equilibrium between the viscosity of the cytoplasm and the nucleoid length so that the propensity for protein aggregates to be at the poles is maximized. Further, these results indicate that the spatial distribution of protein aggregates is temperature dependent.

Given the cell lengths (Figure 5.1 (A)) and assuming that the nucleoids' centers are aligned with the cell center, the distance (relative to the cell's length) of the border of the nucleoids furthest away from the midcell ranges from 0.2 to 0.3. Thus, the distance between a cell's extremity and the nearest outer border of the nucleoid ranges from 0.10 to 0.15. Interestingly, the distribution of distances of the aggregates have modes with very similar values, indicating that, unlike Z-rings (which tend to locate as near as possible to their ideal position), most aggregates tend to be in between the cell's ex-

tremity and the nucleoid's outer border, which, given the curvature of the cell pole, is likely to be the point of least energy.

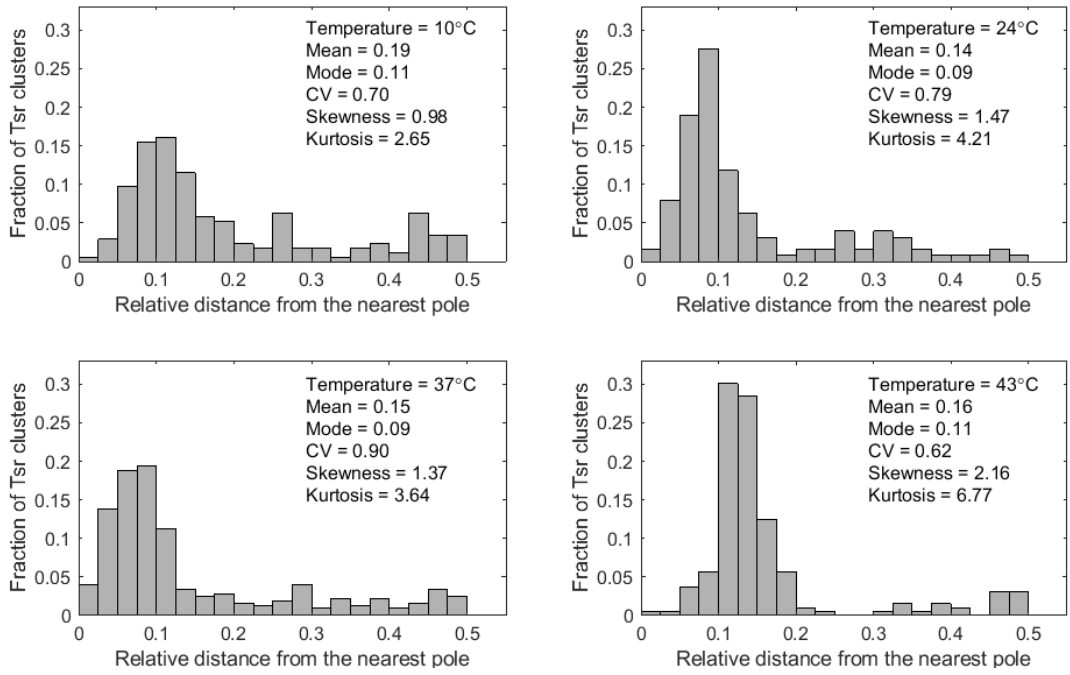

Figure 5.4. *Distribution of distances (relative to the cell length) between the Tsr clusters' position and their nearest cell pole for 10 °C, 24 °C, 37 °C and 43 °C and for more than 100 cells in each temperature. Each graph has an inset with the temperature and information about the distributions, namely their mean, mode, coefficient of variation (CV), skewness and kurtosis.*

Figure 5.4 shows that the distribution of distances of Tsr clusters to the nearest cell poles is similar to those of protein aggregates (although the minimum mean occurs at 24 °C). The modes also suggest that the curvature of the cell's end prevents the clusters to localize nearer the extremity of the pole. However, for reasons yet unknown, the coefficients of variation (CVs) are higher than the CVs of the distributions of protein aggregates, maximizing at 37 °C. Note that as the cells measured did not have Tol-Pal complexes, this diffusion-and-capture mechanism should not be responsible for these values. Instead, the results might be due to mechanisms (other than nucleoid occlusion and diffusion-and-capture) that are also both responsible for positioning chemotaxis networks and temperature-dependent.

We have seen that both the nucleoid's morphology and the spatial distribution of Z-rings, protein aggregates and Tsr clusters change with temperature. The congruence between the variations in the spatial distributions and nucleoid's size and positioning, suggest that the nucleoid affects the efficiency of the placement of these macromolecules. Therefore, the next step is to investigate the existence of a correlation between the nucleoid(s) length and the positioning of these components.

5.3 Correlation of the spatial distributions of cellular components with the nucleoid's morphology

To find a correlation between the nucleoid's morphology and the spatial distributions of Z-rings, protein aggregates and Tsr clusters, we explored how they changed with temperature.

Apart from nucleoid exclusion, the placement may also rely on other mechanisms, specific to each component. Since these may also change differently with temperature, they may create specific positioning patterns for each component.

Though the distributions of distances differ between components, there is visible trend that is common to the three components studied (Figures 5.2, 5.3 and 5.4), e.g. how the tails of the distribution change with temperature. These changes tend to follow the changes in the nucleoid(s) length and/or the distance between the nucleoids. Namely, the tail of the distribution of distances for the Z-ring decreases from 10 °C to 37 °C, increasing again at 43 °C, which is the same behavior that the distance between nucleoids has with temperature changes. This is expected, when considering that a bigger distance between nucleoids provides a wide space for the Z-ring to form. As for the tails in the distributions of distances of aggregates and Tsr clusters, they tend to decrease with increasing temperature, matching the changes observed in the nucleoid's length with increasing temperature. This is also expected, when considering that smaller nucleoids create a weaker occlusion effect, which increases the degree of "leakiness" in the macromolecules from the poles, which is expected to increase the tails of the distributions of distances seen in Figure 5.3 and 5.4.

Since kurtosis (K) measures the prominence of the tail of a distribution, we searched for correlations between K of the distribution of distances for each temperature and the mean of the nucleoid's length (for protein aggregates and Tsr clusters) or the distance between nucleoids (for Z-rings). If these correlations exist and are significant, then it can be concluded that it is very likely that the nucleoid's morphology affects the placement of cellular components.

Figure 5.5 shows the correlation between K of the distributions of distances of the Z-ring from midcell and the mean distance between nucleoids at each temperature. Furthermore, the red line, which represents the best linear fit between the results at four temperature conditions, suggests that there is a statistically significant correlation between these two measures (p-value of the linear least-squares regression fit is 0.01), further supporting that the nucleoid(s) significantly affect the placement of the Z-ring.

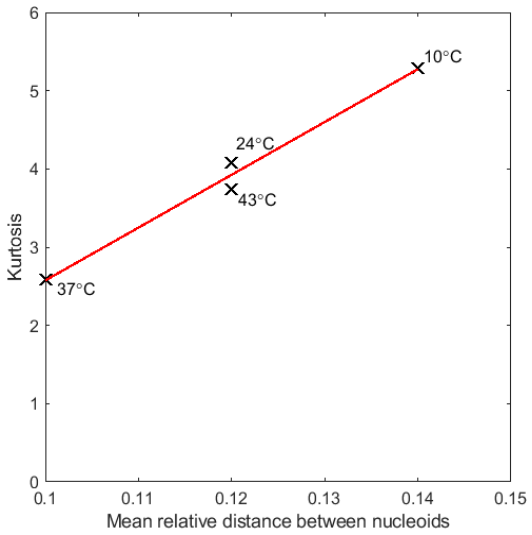

Figure 5.5. *Correlation between the kurtosis of the distributions of distances (relative to the cell length) from the Z-ring's position to the midcell and the mean distance from the inner border of the nucleoids. The data for both measures was retrieved from cells with two nucleoids for the temperatures of 10 °C, 24 °C, 37 °C and 43 °C (shown near each correspondent data point). The solid red line represents the best linear fit found by the least-squares regression fitting method, which has a p-value of 0.01.*

Figure 5.6 shows the correlation between K of the distributions of distances for the protein aggregates and the mean nucleoid length for each temperature. As in Figure 5.5, the red line is the best linear fit between the data points (p-value of 0.09), indicating that there is a statistically significant correlation between these two measures and, thus, that the nucleoid affects the spatial positioning of protein aggregates.

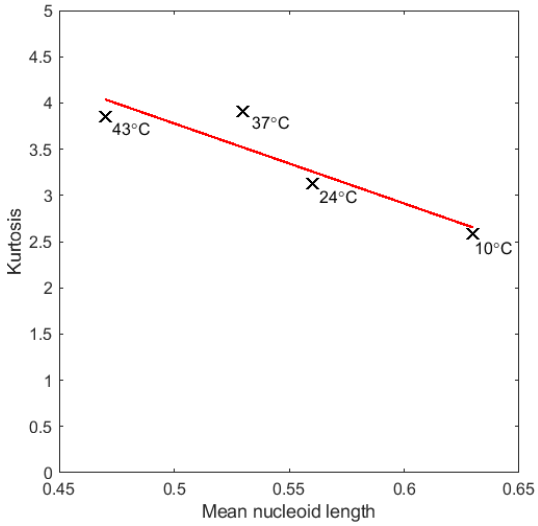

Figure 5.6. *Correlation between the kurtosis of the distributions of distances (relative to the cell length) from the protein aggregates' position to the nearest cell pole and the mean length of the nucleoid. The data for both measures was retrieved from cells with only one nucleoid for the temperatures of 10 °C, 24 °C, 37 °C and 43 °C (shown near each correspondent data point). The solid red line represents the best linear fit found by the least-squares regression fitting method, which has a p-value of 0.09.*

Finally, Figure 5.7 shows the correlation between K of the distributions of distances for the Tsr clusters and the mean nucleoid length at each temperature. However, the best linear fit for the data points (red line), does not allow the rejection of the hypothesis of no correlation between K and the nucleoid's length, since the p-value is 0.13 (thus, higher than 0.1). This lack of statistically significant correlation might be due to insufficient data or the existence of another positioning mechanism. Particularly, as mentioned in section 3.1.3, the matching curvatures of the cell poles and the chemotaxis clusters could be a contributing reason for the chemotaxis network preference for the poles. This common property of chemotaxis clusters and cell poles might decrease the sensitivity of the cluster's location to changing temperatures (when compared to other macromolecules that locate at the poles, such as protein aggregates).

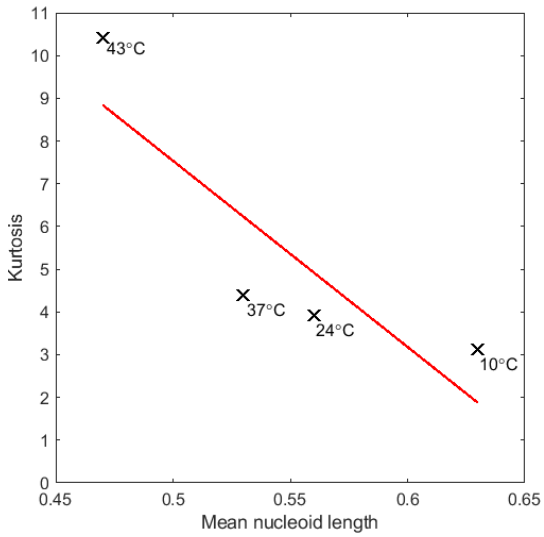

Figure 5.7. *Correlation between the kurtosis of the distributions of distances (relative to the cell length) from the Tsr clusters' position to the nearest cell pole and the mean length of the nucleoid. The data for both measures was retrieved from cells with only one nucleoid for the temperatures of 10 °C, 24 °C, 37 °C and 43 °C (shown near each correspondent data point). The solid red line represents the best linear fit found by the least-squares regression fitting method, which has a p-value of 0.13, which does not allow to conclude that there is a linear correlation between these two measures.*

Given the significant linear correlation between the nucleoid's morphology and the cellular components studied, apart from Tsr clusters (whose p-value is 0.13), it can be assumed that the nucleoid affects the spatial distribution of these components. Next, we investigate to which extend temperature affects the effectiveness of the placement of the components by the nucleoids.

5.4 Efficiency and robustness in the positioning of cellular components

We quantified the efficiency for each placement process at different temperature, using equations (4.1), (4.2) and (4.3). The results were analyzed taking into consideration how the nucleoid's biophysical parameters change within each temperature condition. These efficiencies are shown in Figure 5.8.

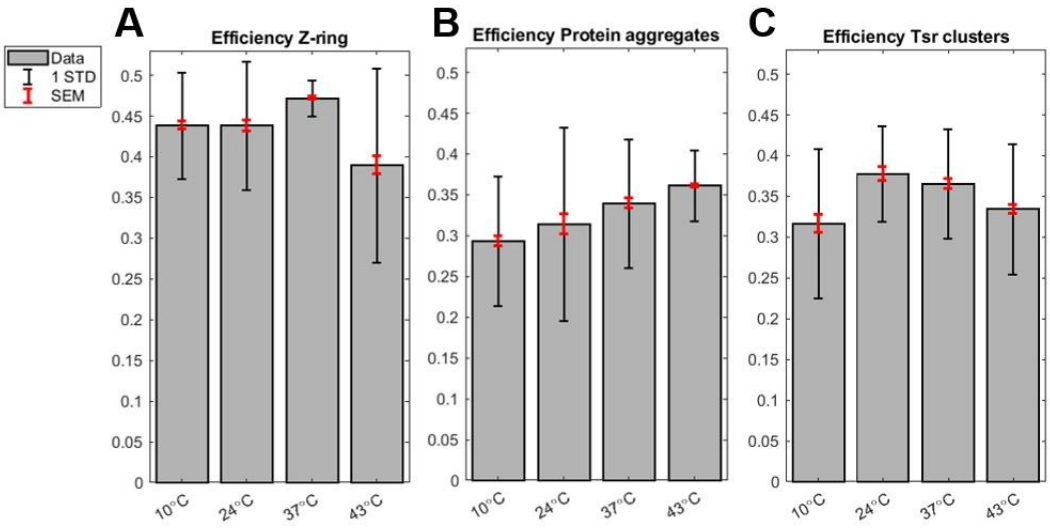

Figure 5.8. *Efficiency for the placement of each cellular component for different temperatures. (A) Efficiency for the placement of the Z-ring for 10 °C, 24 °C, 37 °C and 43 °C. (B) Efficiency for the placement of protein aggregates for 10 °C, 24 °C, 37 °C and 43 °C. (C) Efficiency for the placement of the Tsr clusters for 10 °C, 24 °C, 37 °C and 43 °C. In all bar graphs, the grey bars correspond to the mean efficiency of placements for the correspondent temperature, the black line corresponds to one standard deviation (which provides information on the single-cell variability) and the red line corresponds to the standard error of the mean obtained by bootstrapping (which provides information on the population variability).*

From Figure 5.8, temperature does not affect the efficiency of the placement of the three cellular components similarly. Even though this could be expected for Z-rings, since it's criteria for ideal location differs from the protein aggregates and the Tsr clusters, the reason for the differences between the protein aggregates and Tsr clusters are less obvious. We hypothesize that the existence of an additional phenomenon that only affects the Tsr clusters but not the protein aggregates. For instance, the clustering of Tsr molecules might differ from the clustering process of nonfunctional proteins, being more/less sensitive to temperature. Also, the size of the protein aggregates and Tsr clusters may differ, causing the nucleoid exclusion phenomenon efficiency to maximize/minimize at different temperatures. Nevertheless, both processes have a minimum efficiency at 10 °C, which is probably due to the increase of cytoplasmic viscosity that occurs at critically low temperatures, which fetters the components' mobility.

Furthermore, the efficiencies in the Z-ring placement at different temperatures follow the same trend as the distances between nucleoids for the same temperature changes, suggesting that the nucleoid affects the efficiency of how the Z-ring is placed in the midcell. Interestingly, the placement of Z-rings is most hampered at higher temperatures. This might be due to perturbations in the clustering process of these proteins at these temperatures.

Using equation (4.4) and the results in the bar graphs in Figure 5.8, we calculated the robustness for these three placement processes. Robustness was found to equal 0.88, 0.93 and 0.94 for the Z-ring, Tsr clusters and protein aggregates positioning, respectively. All are smaller but close to 1, implying that these processes are robust to temperature, with the optimal temperature being 37 °C. Nevertheless, they exhibit differences in how they respond to temperature changes.

Finally, the robustness of each placement process was plotted against their efficiency and, as seen in Figure 5.9, a linear correlation was found (p-value of 0.04). We conclude that, the more robust a process is, the less efficiency it has in optimal conditions, suggesting a tradeoff between these two measures of success (within this range of temperature conditions).

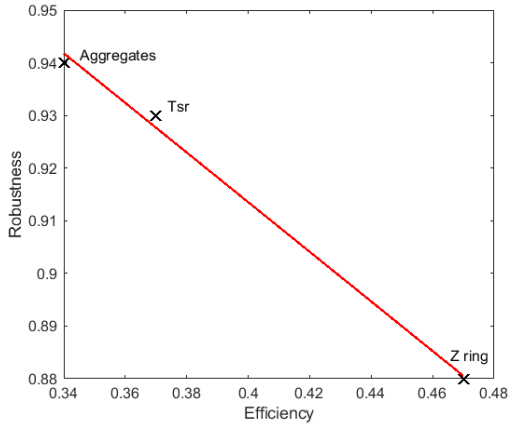

Figure 5.9. *Correlation between the robustness of a process and its efficiency. The robustness was calculated using the equation (5.4) for the nonoptimal temperatures of 10 °C, 24 °C and 43 °C and the efficiency was quantified using the equations (5.1), (5.2) and (5.3) for the optimal temperature of 37 °C. Each process is indicated near its data point. The solid red line represents the best linear fit found by the least-squares regression fitting method, which has a p-value of 0.04, indicating the existence of a negative correlation between the robustness of a process to changes in temperature and its efficiency at an optimal temperature.*

6. CONCLUSIONS AND FUTURE WORK

In this thesis, we assessed the extent to which the nucleoid, as a large and dense cellular structure, aids in various placement processes of other cellular components in *E. coli*, namely Z-rings, protein aggregates and chemotaxis clusters. To do so, we made used of empirical data from microscopy images of the position of the cellular components inside the cell, as well as of the cell and nucleoid length and the distance between nucleoids, following chromosome replication.

To quantify the influence of the nucleoid in these processes, we first defined measures of efficiency of the processes at optimal temperature and their robustness to shifts to nonoptimal temperatures. The formulas make use of the component's distance from its (assumed) ideal position. The robustness — that is, the ability of a process to remain efficient to changing, suboptimal conditions — was defined using the fold change of efficiency between the nonoptimal temperatures of 10 °C, 24 °C and 43 °C and the optimal temperature of 37 °C.

Next, we investigated from empirical data how the nucleoid's morphology and the spatial distribution the components changed with changing temperatures. Regarding the nucleoid's morphology, there were visible changes, as its length decreased with increasing temperatures and the space between replicated nucleoids was minimal at 37 °C.

Next, we assessed the distributions of distances from the ideal position for each component and each temperature condition. For the Z-ring, the changes in distances from the cell center for different temperatures, namely the minimal mean distance at 37 °C, could be explained by the changes in the distance between the nucleoids. For protein aggregates, the response to temperature of the nucleoid (through nucleoid exclusion) and the cytoplasm (whose viscosity hampers the aggregates' mobility) could explain the changes in the mean (minimal at 37 °C) and overall shape of the distributions. Finally, for Tsr clusters, though some changes can be explained by the nucleoid's length, there are several parameters (such as the CV) that suggest the existence of another temperature-dependent mechanism that affects the clusters' positioning. Furthermore, in both the protein aggregates and Tsr clusters, the propensity to remain in the space in between the nucleoid's outer border and the cell extreme (unlike Z-rings, which tend

to remain as close as possible from midcell) can be explained by the curvature of the cell poles.

Having found differences in the distributions for different temperatures, which were consistent with changes in the nucleoids morphology's, we proceeded to ascertain whether the changes observed in the distributions of distances — particularly in the kurtosis — were correlated to the changes in either the nucleoid's length of the distance between nucleoids. Generally, such linear correlations between the positioning of the components and the morphology of the nucleoid(s) further suggest that the nucleoid, through nucleoid exclusion, is a source of spatial organization of macromolecules inside *E. coli* cells.

Next, given the evidence that the nucleoid — through changes in its morphology caused by temperature shifts — affects the placement processes, we calculated the efficiency (for each temperature) and robustness (to changing temperatures) of each process. Overall, the changes in efficiency for increasing temperature differs between the cellular components observed. The efficiency in the Z-rings increases when the distance between nucleoids is shorter. The same does not occurs for the other macromolecules. Though the decreasing cytoplasmic viscosity in increasing temperatures can explain the efficiency in the protein aggregates' placement and the minimal efficiency in the placement of Tsr clusters at 10 °C, it cannot explain the overall behavior of the efficiencies of positioning of the Tsr clusters. The processes were also found to be robust (0.88, 0.93 and 0.94 for Z-rings, protein aggregates and Tsr clusters, respectively). Finally, the negative linear correlation found between robustness and efficiency seem to suggest a tradeoff between these measures Even though such relationship is commonly seen in various phenomena, it was not naturally expected in this particular case since more than one variable affects the positioning of these components and the variables other than the nucleoid do not affect all three components observed.

In the future, we aim to conduct further research to investigate the underlying reasons for observed differences in how the efficiency of these processes' changes with temperature. Namely, if these differences are a result of the different properties of the components themselves — such as in shape and size — or are due to the existence of additional mechanisms that influence their spatial organization. It will also be interesting to see how other cellular components are affected by nucleoid exclusion.

This thesis gathered a wide amount of empirical data on the influence of nucleoid exclusion on the internal spatial organization of *E. coli* cells. Furthermore, we proposed new means of evaluating the success in the placement processes, such as efficiency

and robustness, which are not depend on specific characteristics of each component, so as to draw general conclusions on the nucleoid occlusion phenomenon. It also allows us to compare the placement processes based on the nucleoid, which may contribute to identifying the existence of additional contributing mechanisms in the case of specific components.

REFERENCES

[1] S. Shashkova and M. C. Leake, “Single-molecule fluorescence microscopy review: shedding new light on old problems,” *Biosci. Rep.*, vol. 37, no. 4, p. BSR20170031, 2017.

[2] B. Alberts, A. Johnson, J. Lewis, M. Raff, K. Roberts, and P. Walter, *Molecular Biology of the Cell*, 5th ed. Garland Science, 2008.

[3] D. Huh and J. Paulsson, “Random partitioning of molecules at cell division,” *Proc. Natl. Acad. Sci.*, vol. 108, no. 36, pp. 15004–15009, 2011.

[4] A. B. Lindner, R. Madden, A. Demarez, E. J. Stewart, and F. Taddei, “Asymmetric segregation of protein aggregates is associated with cellular aging and rejuvenation,” *Proc. Natl. Acad. Sci.*, vol. 105, no. 8, pp. 3076–3081, 2008.

[5] A. Gupta, J. Lloyd-Price, R. Neeli-Venkata, S. M. D. Oliveira, and A. S. Ribeiro, “In Vivo Kinetics of Segregation and Polar Retention of MS2-GFP-RNA Complexes in *Escherichia coli*,” *Biophys. J.*, vol. 106, no. 9, pp. 1928–1937, May 2014.

[6] R. Neeli-Venkata, S. Startceva, T. Annila, and A. S. Ribeiro, “Polar Localization of the Serine Chemoreceptor of *Escherichia coli* Is Nucleoid Exclusion-Dependent,” *Biophys. J.*, vol. 111, no. 11, pp. 2512–2522, 2016.

[7] R. Neeli-Venkata, A. Martikainen, A. Gupta, N. Gonçalves, J. Fonseca, and A. S. Ribeiro, “Robustness of the Process of Nucleoid Exclusion of Protein Aggregates in *Escherichia coli*,” *J. Bacteriol.*, vol. 198, no. 6, pp. 898–906, Mar. 2016.

[8] R. Neeli-Venkata *et al.*, “The precision of the symmetry in Z-ring placement in *Escherichia coli* is hampered at critical temperatures,” *Phys. Biol.*, vol. 15, no. 5, p. 056002, 2018.

[9] J. K. Fisher, A. Bourniquel, G. Witz, B. Weiner, M. Prentiss, and N. Kleckner, “Four-Dimensional Imaging of *E. coli* Nucleoid Organization and Dynamics in Living Cells,” *Cell*, vol. 153, no. 4, pp. 882–895, May 2013.

[10] M. B. Elowitz, A. J. Levine, E. D. Siggia, and P. S. Swain, “Stochastic Gene

Expression in a Single Cell," *Science.*, vol. 297, no. 5584, pp. 1183–1186, Aug. 2002.

[11] M. Acar, J. T. Mettetal, and A. Van Oudenaarden, "Stochastic switching as a survival strategy in fluctuating environments," *Nat. Genet.*, vol. 40, no. 4, pp. 471–475, 2008.

[12] T. Wang and M. J. Dunlop, "Controlling and exploiting cell-to-cell variation in metabolic engineering," *Curr. Opin. Biotechnol.*, vol. 57, pp. 10–16, 2018.

[13] S. T. Shulman, H. C. Friedmann, and R. H. Sims, "Theodor Escherich: The First Pediatric Infectious Diseases Physician?," *Clin. Infect. Dis.*, vol. 45, no. 8, pp. 1025–1029, 2007.

[14] B. Volkmer and M. Heinemann, "Condition-Dependent cell volume and concentration of *Escherichia coli* to facilitate data conversion for systems biology modeling," *PLoS One*, vol. 6, no. 7, p. e23126, 2011.

[15] M. A. Savageau, "*Escherichia coli* Habitats, Cell Types, and Molecular Mechanisms of Gene Control," *Am. Nat.*, vol. 122, no. 6, pp. 732–744, 1983.

[16] S. B. Zimmerman and L. D. Murphy, "Macromolecular crowding and the mandatory condensation of DNA in bacteria," *FEBS Lett.*, vol. 390, no. 3, pp. 245–248, 1996.

[17] R. J. Ellis, "Macromolecular crowding: obvious but underappreciated," *Trends Biochem. Sci.*, vol. 26, no. 10, pp. 597–604, 2001.

[18] M. B. Elowitz *et al.*, "Protein Mobility in the Cytoplasm of *Escherichia coli*," *Society*, vol. 181, no. 1, pp. 197–203, 1999.

[19] I. Golding and E. C. Cox, "Physical nature of bacterial cytoplasm," *Phys. Rev. Lett.*, vol. 96, no. 9, pp. 14–17, 2006.

[20] L. Niu and J. Yu, "Investigating Intracellular Dynamics of FtsZ Cytoskeleton with Photoactivation Single-Molecule Tracking," *Biophys. J.*, vol. 95, no. 4, pp. 2009–2016, Aug. 2008.

[21] B. P. English, A. Sanamrad, S. Tankov, V. Hauryliuk, and J. Elf, "Tracking of individual freely diffusing fluorescent protein molecules in the bacterial cytoplasm," *Arxiv*, pp. 1–30, Mar. 2010.

[22] S. Bakshi, B. P. Bratton, and J. C. Weisshaar, "Subdiffraction-Limit Study of Kaede Diffusion and Spatial Distribution in Live *Escherichia coli*," *Biophys. J.*, vol. 101, no. 10, pp. 2535–2544, Nov. 2011.

[23] A. S. Coquel *et al.*, “Localization of Protein Aggregation in *Escherichia coli* Is Governed by Diffusion and Nucleoid Macromolecular Crowding Effect,” *PLoS Comput. Biol.*, vol. 9, no. 4, p. e1003038, 2013.

[24] “Stokes–Einstein equation - Oxford Reference,” 2014. [Online]. Available: http://www.oxfordreference.com/view/10.1093/acref/9780199651450.001.0001/acref-9780199651450-e-2777?rskey=1ha0oP&result=2. [Accessed: 15-May-2019].

[25] E. O. Puchkov, “Intracellular viscosity: Methods of Measurement and Role in Metabolism,” *Biochem. Suppl. Ser. A Membr. Cell Biol.*, vol. 7, no. 4, pp. 270–279, 2013.

[26] S. Bolsover, J. Hyams, E. Shephard, H. White, and C. A Weidemann, *Cell Biology: A Short Course*, 2nd ed. John Wiley & Sons, Inc., 2004.

[27] X. Wang, P. M. Llopis, and D. Z. Rudner, “Organization and segregation of bacterial chromosomes,” *Nat. Rev. Genet.*, vol. 14, no. 3, pp. 191–203, 2013.

[28] R. P. C. Driessen *et al.*, “Effect of Temperature on the Intrinsic Flexibility of DNA and Its Interaction with Architectural Proteins,” *Biochemistry*, vol. 53, no. 41, pp. 6430–6438, Oct. 2014.

[29] X. Wang, X. Liu, C. Possoz, and D. J. Sherratt, “The two *Escherichia coli* chromosome arms locate to separate cell halves,” *Genes Dev.*, vol. 20, no. 13, pp. 1727–1731, 2006.

[30] L. Dewachter, N. Verstraeten, M. Fauvart, and J. Michiels, “An integrative view of cell cycle control in *Escherichia coli*,” *FEMS Microbiol. Rev.*, vol. 42, no. 2, pp. 116–136, 2018.

[31] S. Jun and A. Wright, “Entropy as the driver of chromosome segregation,” *Nat. Rev. Microbiol.*, vol. 8, no. 8, pp. 600–607, Aug. 2010.

[32] N. J. Kuwada, K. C. Cheveralls, B. Traxler, and P. A. Wiggins, “Mapping the driving forces of chromosome structure and segregation in *Escherichia coli*,” *Nucleic Acids Res.*, vol. 41, no. 15, pp. 7370–7377, 2013.

[33] K. Skarstad, H. B. Steen, and E. Boye, “Cell cycle Parameters of Slowly growing Escherichia coli B/r studied by Flow Cytometry,” *J. Bacteriol.*, vol. 154, no. 2, pp. 656–662, 1983.

[34] H. Tran, “Environment-sensing Mechanisms of Gene Expression and their Effects on the Dynamics of Genetic Circuits across Cell Generations,” Tampere

University of Technology, 2016.

[35] E. J. Stewart, R. Madden, G. Paul, and F. Taddei, “Aging and Death in an oOrganism that Reproduces by Morphologically Symmetric Division,” *PLoS Biol.*, vol. 3, no. 2, p. e45, 2005.

[36] E. Harry, L. Monahan, and L. Thompson, “Bacterial Cell Division: The Mechanism and Its Precison,” *Int. Rev. Cytol.*, vol. 253, no. 06, pp. 27–94, 2006.

[37] N. W. Goehring and J. Beckwith, “Diverse paths to midcell: Assembly of the bacterial cell division machinery,” *Curr. Biol.*, vol. 15, no. 13, pp. R514–R526, 2005.

[38] C. Fraipont *et al.*, “The integral membrane FtsW protein and peptidoglycan synthase PBP3 form a subcomplex in Escherichia coli,” *Microbiology*, vol. 157, no. 1, pp. 251–259, 2011.

[39] I. Grainge, “FtsK - a bacterial cell division checkpoint?,” *Mol. Microbiol.*, vol. 78, no. 5, pp. 1055–1057, 2010.

[40] J. Lowe and L. A. Amos, “Crystal structure of the bacterial cell-division protein FtsZ,” *Nature*, vol. 391, pp. 203–206, 1998.

[41] D. W. Adams and J. Errington, “Bacterial cell division: Assembly, maintenance and disassembly of the Z ring,” *Nat. Rev. Microbiol.*, vol. 7, no. 9, pp. 642–653, 2009.

[42] X. Ma, D. W. Ehrhardt, and W. Margolin, “Colocalization of cell division proteins FtsZ and FtsA to cytoskeletal structures in living Escherichia coli cells by using green fluorescent protein,” *Proc. Natl. Acad. Sci.*, vol. 93, no. 23, pp. 12998–13003, 1996.

[43] B. Shen and J. Lutkenhaus, “The conserved C-terminal tail of FtsZ is required for the septal localization and division inhibitory activity of MinCC /MinD,” *Mol. Microbiol. Microbiol*, vol. 72, no. 2, pp. 410–424, 2009.

[44] S. Pichoff and J. Lutkenhaus, “Unique and overlapping roles for ZipA and FtsA in septal ring assembly in Escherichia coli,” *EMBO J.*, vol. 21, no. 4, pp. 685–693, 2002.

[45] V. M. Hernández-Rocamora *et al.*, “MinC protein shortens FtsZ protofilaments by preferentially interacting with GDP-bound subunits,” *J. Biol. Chem.*, vol. 288, no. 34, pp. 24625–24635, 2013.

[46] D. M. Raskin and P. A. J. de Boer, “Rapid pole-to-pole oscillation of a protein

required for directing division to the middle of Escherichia coli," *Proc. Natl. Acad. Sci.*, vol. 96, no. 9, pp. 4971–4976, Apr. 1999.

[47] Z. Hu and J. Lutkenhaus, "Topological regulation of cell division in Escherichia coli involves rapid pole to pole oscillation of the division inhibitor MinC under the control of MinD and MinE," *Mol. Microbiol.*, vol. 34, no. 1, pp. 82–90, 1999.

[48] A. G. Vecchiarelli *et al.*, "Membrane-bound MinDE complex acts as a toggle switch that drives Min oscillation coupled to cytoplasmic depletion of MinD," *Proc. Natl. Acad. Sci.*, vol. 113, no. 11, pp. E1479–E1488, 2016.

[49] T. G. Bernhardt and P. A. J. de Boer, "SlmA, a Nucleoid-Associated, FtsZ Binding Protein Required for Blocking Septal Ring Assembly over Chromosomes in *E. coli*," *Mol. Cell*, vol. 18, no. 5, pp. 555–564, May 2005.

[50] S. Du and J. Lutkenhaus, "SlmA Antagonism of FtsZ Assembly Employs a Two-pronged Mechanism like MinCD," *PLoS Genet.*, vol. 10, no. 7, p. e1004460, 2014.

[51] H. Cho, H. R. McManus, S. L. Dove, and T. G. Bernhardt, "Nucleoid occlusion factor SlmA is a DNA-activated FtsZ polymerization antagonist," *Proc. Natl. Acad. Sci.*, vol. 108, no. 9, pp. 3773–3778, 2011.

[52] N. K. Tonthat *et al.*, "Molecular mechanism by which the nucleoid occlusion factor, SlmA, keeps cytokinesis in check," *EMBO J.*, vol. 30, no. 1, pp. 154–164, 2011.

[53] X. Wang, C. Possoz, and D. J. Sherratt, "Dancing around the divisome: asymmetric chromosome segregation in Escherichia coli," *Genes Dev.*, vol. 19, no. 19, pp. 2367–2377, 2005.

[54] M. W. Bailey, P. Bisicchia, B. T. Warren, D. J. Sherratt, and J. Männik, "Evidence for Divisome Localization Mechanisms Independent of the Min System and SlmA in Escherichia coli," *PLoS Genet.*, vol. 10, no. 8, p. e1004504, 2014.

[55] O. Espéli *et al.*, "A MatP-divisome interaction coordinates chromosome segregation with cell division in *E. coli*," *EMBO J.*, vol. 31, no. 14, pp. 3198–3211, 2012.

[56] E. Galli and K. Gerdes, "Spatial resolution of two bacterial cell division proteins: ZapA recruits ZapB to the inner face of the Z-ring," *Mol. Microbiol.*, vol. 76, no. 6, pp. 1514–1526, 2010.

[57] J. Buss, C. Coltharp, G. Shtengel, X. Yang, H. Hess, and J. Xiao, “A Multi-layered Protein Network Stabilizes the Escherichia coli FtsZ-ring and Modulates Constriction Dynamics,” *PLOS Genet.*, vol. 11, no. 4, p. e1005128, 2015.

[58] Y. Taniguchi *et al.*, “Quantifying *E. coli* Proteome and Transcriptome with Single-Molecule Sensitivity in Single Cells,” *Science.*, vol. 329, no. 5991, pp. 533–538, Jul. 2010.

[59] D. Huh and J. Paulsson, “Non-genetic heterogeneity from stochastic partitioning at cell division,” *Nat. Genet.*, vol. 43, no. 2, pp. 95–100, Feb. 2011.

[60] J. Mondal, B. P. Bratton, Y. Li, A. Yethiraj, and J. C. Weisshaar, “Entropy-Based Mechanism of Ribosome-Nucleoid Segregation in *E. coli* Cells,” *Biophys. J.*, vol. 100, no. 11, pp. 2605–2613, Jun. 2011.

[61] Q. Chai *et al.*, “Organization of ribosomes and nucleoids in escherichia coli cells during growth and in quiescence,” *J. Biol. Chem.*, vol. 289, no. 16, pp. 11342–11352, 2014.

[62] M. Castellana, S. Hsin-Jung Li, and N. S. Wingreen, “Spatial organization of bacterial transcription and translation,” *Proc. Natl. Acad. Sci.*, vol. 113, no. 33, pp. 9286–9291, Aug. 2016.

[63] H. F. Lodish *et al.*, *Molecular Cell Biology*, 6th ed. W. H. Freeman, 2008.

[64] F. U. Hartl, “Molecular chaperones in cellular protein folding,” *Nature*, vol. 381, no. 6583, pp. 571–580, Jun. 1996.

[65] F. U. Hartl, A. Bracher, and M. Hayer-Hartl, “Molecular chaperones in protein folding and proteostasis,” *Nature*, vol. 475, no. 7356, pp. 324–332, Jul. 2011.

[66] S. Wickner, M. R. Maurizi, and S. Gottesman, “Posttranslational Quality Refolding , Control : Proteins Folding , Degrading,” *Adv. Sci.*, vol. 286, no. 5446, pp. 1888–1893, 1999.

[67] A. L. Goldberg, “Degradation of Abnormal Proteins in Escherichia coli (protein breakdown/protein structure/mistranslation/amino acid analogs/puromycin).,” *Proc. Natl. Acad. Sci. U. S. A.*, vol. 69, no. 2, pp. 422–6, Feb. 1972.

[68] J. Tyedmers, A. Mogk, and B. Bukau, “Cellular strategies for controlling protein aggregation,” *Nat. Rev. Mol. cell Biol.*, vol. 11, no. 11, pp. 777–788, Nov. 2010.

[69] Y. E. Kim, M. S. Hipp, A. Bracher, M. Hayer-Hartl, and F. Ulrich Hartl, “Molecular Chaperone Functions in Protein Folding and Proteostasis,” *Annu. Rev. Biochem.*, vol. 82, no. 1, pp. 323–355, 2013.

[70] N. G. Bednarska, J. Schymkowitz, F. Rousseau, and J. Van Eldere, “Protein aggregation in bacteria: The thin boundary between functionality and toxicity,” *Microbiology*, vol. 159, pp. 1795–1806, 2013.

[71] H. C. Berg and D. A. Brown, “Chemotaxis in Escherichia coli analysed by three-dimensional tracking,” *Nature*, vol. 239, no. 5374, pp. 500–504, 1972.

[72] V. Sourjik and N. S. Wingreen, “Responding to chemical gradients: Bacterial chemotaxis,” *Curr. Opin. Cell Biol.*, vol. 24, no. 2, pp. 262–268, 2012.

[73] J. S. Parkinson, P. Ames, and C. A. Studdert, “Collaborative signaling by bacterial chemoreceptors,” *Curr. Opin. Microbiol.*, vol. 8, no. 2, pp. 116–121, Apr. 2005.

[74] V. Sourjik and J. P. Armitage, “Spatial organization in bacterial chemotaxis,” *EMBO J.*, vol. 29, no. 16, pp. 2724–2733, 2010.

[75] G. L. Hazelbauer, J. J. Falke, and J. S. Parkinson, “Bacterial chemoreceptors: high-performance signaling in networked arrays,” *Trends Biochem. Sci.*, vol. 33, no. 1, pp. 9–19, 2008.

[76] D. Greenfield *et al.*, “Self-Organization of the Escherichia coli Chemotaxis Network Imaged with Super-Resolution Light Microscopy,” *PLoS Biol.*, vol. 7, no. 6, p. e1000137, Jun. 2009.

[77] Maddock and L. Shapiro, “Polar location of the chemoreceptor complex in the Escherichia coli cell,” *Science.*, vol. 259, no. 5102, pp. 1717 LP – 1723, Mar. 1993.

[78] P. Zhang, C. M. Khursigara, L. M. Hartnell, and S. Subramaniam, “Direct visualization of Escherichia coli chemotaxis receptor arrays using cryo-electron microscopy,” *Proc. Natl. Acad. Sci.*, vol. 104, no. 10, pp. 3777–3781, 2007.

[79] S. Stylianidou, N. J. Kuwada, and P. A. Wiggins, “Cytoplasmic Dynamics Reveals Two Modes of Nucleoid-Dependent Mobility.,” *Biophys. J.*, vol. 107, no. 11, pp. 2684–2692, 2014.

[80] F. J. Trueba, “On the Precision and Accuracy Achieved by Escherichia coli Cells at Fission About their Middle,” *Arch. Microbiol.*, vol. 131, no. 1, pp. 55–59, 1982.

[81] S. M. Sullivan and J. R. Maddock, “Bacterial division: Finding the dividing line,” *Curr. Biol.*, vol. 10, no. 6, pp. R249–R252, 2000.

[82] A. Gupta, J. Lloyd-Price, S. M. D. Oliveira, O. Yli-Harja, A.-B. Muthukrishnan, and A. S. Ribeiro, “Robustness of the division symmetry in Escherichia coli and

functional consequences of symmetry breaking," *Phys. Biol.*, vol. 11, no. 6, p. 066005, Nov. 2014.

[83] L. Partridge and N. H. Barton, "Optimally, mutation and the evolution of ageing," *Nature*, vol. 362, pp. 305–311, 1993.

[84] J. Lloyd-Price *et al.*, "Asymmetric Disposal of Individual Protein Aggregates in Escherichia coli, One Aggregate at a Time," *J. Bacteriol.*, vol. 194, no. 7, pp. 1747–1752, 2012.

[85] S. Gordon, J. Rech, D. Lane, and A. Wright, "Kinetics of plasmid segregation in Escherichia coli," *Mol. Microbiol.*, vol. 51, no. 2, pp. 461–469, Feb. 2004.

[86] Z. Schuss, A. Singer, and D. Holcman, "The narrow escape problem for diffusion in cellular microdomains," *Proc. Natl. Acad. Sci.*, vol. 104, no. 41, pp. 16098–16103, 2007.

[87] D. Oh, Y. Yu, H. Lee, B. L. Wanner, and K. Ritchie, "Dynamics of the Serine Chemoreceptor in the Escherichia coli Inner membrane: A High-Speed Single-Molecule Tracking Study," *Biophys. J.*, vol. 106, no. 1, pp. 145–153, 2014.

[88] S. Thiem, D. Kentner, and V. Sourjik, "Positioning of chemosensory clusters in *E. coli* and its relation to cell division," *EMBO J.*, vol. 26, no. 6, pp. 1615–1623, Mar. 2007.

[89] W. Draper and J. Liphardt, "Origins of chemoreceptor curvature sorting in Escherichia coli," *Nat. Commun.*, vol. 8, p. 14838, Mar. 2017.

[90] C. W. Jones and J. P. Armitage, "Positioning of bacterial chemoreceptors," *Trends Microbiol.*, vol. 23, no. 5, pp. 247–256, 2015.

[91] G. Laloux and C. Jacobs-Wagner, "How do bacteria localize proteins to the cell pole?," *J. Cell Sci.*, vol. 127, no. 1, pp. 11–19, Jan. 2014.

[92] T. M. A. Santos, T. Y. Lin, M. Rajendran, S. M. Anderson, and D. B. Weibel, "Polar localization of Escherichia coli chemoreceptors requires an intact Tol-Pal complex," *Mol. Microbiol.*, vol. 92, no. 5, pp. 985–1004, 2014.

[93] A. Walburger, C. Lazdunski, and Y. Corda, "The Tol/Pal system function requires an interaction between the C-terminal domain of TolA and the N-terminal domain of TolB," *Mol. Microbiol.*, vol. 44, no. 3, pp. 695–708, 2002.

[94] A. Gupta, J. Lloyd-Price, and A. S. Ribeiro, "In silico analysis of division times of Escherichia coli populations as a function of the partitioning scheme of non-functional proteins," *In Silico Biol.*, vol. 12, no. 2012–2014, pp. 9–21, 2015.

[95] B. R. Parry, I. V. Surovtsev, M. T. Cabeen, C. S. O'Hern, E. R. Dufresne, and C. Jacobs-Wagner, "The Bacterial Cytoplasm Has Glass-like Properties and Is Fluidized by Metabolic Activity," *Cell*, vol. 156, no. 1–2, pp. 183–194, Jan. 2014.

[96] J. Spitzer, "From Water and Ions to Crowded Biomacromolecules: In Vivo Structuring of a Prokaryotic Cell," *Microbiol. Mol. Biol. Rev.*, vol. 75, no. 3, pp. 491–506, Sep. 2011.

[97] J. Spitzer and B. Poolman, "The Role of Biomacromolecular Crowding, Ionic Strength, and Physicochemical Gradients in the Complexities of Life's Emergence," *Microbiol. Mol. Biol. Rev.*, vol. 73, no. 2, pp. 371–388, 2009.

[98] T. E. Shehata and A. G. Marr, "Effect of temperature on the size of Escherichia coli cells," *J. Bacteriol.*, vol. 124, no. 2, pp. 857–862, 1975.

[99] A. Farewell and F. C. Neidhardt, "Effect of Temperature on In Vivo Protein Synthetic Capacity in Escherichia coli," *J. Bacteriol.*, vol. 180, no. 17, pp. 4704–4710, 1998.

[100] S. M. D. Oliveira *et al.*, "Increased cytoplasm viscosity hampers aggregate polar segregation in Escherichia coli," *Mol. Microbiol.*, vol. 99, no. 4, pp. 686–699, 2016.

[101] A. Beiser, *Concepts of Modern Physics*, 6th ed. McGraw-Hill, 2003.

[102] J. Kapuscinski, "DAPI: a DNA-specific fluorescent probe," *Biotech. Histochem.*, vol. 70, no. 5, pp. 220–233, 1995.

[103] A. S. Rose, A. R. Bradley, Y. Valasatava, J. M. Duarte, A. Prlić, and P. W. Rose, "PDB ID: 1D30 |NGL viewer: web-based molecular graphics for large complexes," *Bioinformatics*, 01-Nov-2018. [Online]. Available: https://www.rcsb.org/3d-view/1D30. [Accessed: 16-May-2019].

[104] R. Neeli-Venkata, "The Role of Nucleoid Exclusion in the Intracellular Spatial Organization of Escherichia coli," Tampere University of Technology, 2017.

[105] O. Shimomura, F. H. Johnson, and Y. Saiga, "Extraction, Purification and Properties of Aequorin, a Bioluminescent Protein from the Luminous Hydromedusan, Aequorea," *J. Cell. Comp. Physiol.*, vol. 59, no. 3, pp. 223–239, Jun. 1962.

[106] M. Chalfie, Y. Tu, G. Euskirchen, W. W. Ward, and D. C. Prasher, "Green Fluorescent Protein as a Marker for Gene Expression," *Science.*, vol. 263, no. 5148, pp. 802–805, 1994.

[107] R. N. Day and M. W. Davidson, “The fluorescent protein palette: tools for cellular imaging,” *Chem. Soc. Rev.*, vol. 38, no. 10, pp. 2887–2921, 2009.

[108] X. S. Xie, P. J. Choi, G.-W. Li, N. K. Lee, and G. Lia, “Single-Molecule Approach to Molecular Biology in Living Bacterial Cells,” *Annu. Rev. Biophys.*, vol. 37, no. 1, pp. 417–444, Jun. 2008.

[109] A. Gahlmann and W. E. Moerner, “Exploring bacterial cell biology with single-molecule tracking and super-resolution imaging,” *Nat. Rev. Microbiol.*, vol. 12, no. 1, pp. 9–22, 2014.

[110] B. N. G. Giepmans, S. R. Adams, M. H. Ellisman, and R. Y. Tsien, “The Fluorescent Toolbox for Assessing Protein Location and Function,” *Science.*, vol. 312, no. April, pp. 217–224, 2006.

[111] I. Golding and E. C. Cox, “RNA dynamics in live Escherichia coli cells,” *Proc. Natl. Acad. Sci.*, vol. 101, no. 31, pp. 11310–11315, 2004.

[112] C. Keryer-Bibens, C. Barreau, and H. B. Osborne, “Tethering of proteins to RNAs by bacteriophage proteins,” *Biol. Cell*, vol. 100, no. 2, pp. 125–138, Feb. 2008.

[113] I. Golding, J. Paulsson, S. M. Zawilski, and E. C. Cox, “Real-Time Kinetics of Gene Activity in Individual Bacteria,” *Cell*, vol. 123, no. 6, pp. 1025–1036, Dec. 2005.

[114] M. Kandhavelu, A. Häkkinen, O. Yli-Harja, and A. S. Ribeiro, “Single-molecule dynamics of transcription of the lar promoter,” *Phys. Biol.*, vol. 9, no. 2, p. 026004, Apr. 2012.

[115] B. Söderström, K. Mirzadeh, S. Toddo, G. von Heijne, U. Skoglund, and D. O. Daley, “Coordinated disassembly of the divisome complex in Escherichia coli,” *Mol. Microbiol.*, vol. 101, no. 3, pp. 425–438, Aug. 2016.

[116] J. Yu, J. Xiao, X. Ren, K. Lao, and X. S. Xie, “Probing Gene Expression in Live Cells, One Protein Molecule at a Time,” *Science.*, vol. 311, no. 5767, pp. 1600–1603, Mar. 2006.

[117] T. Ha and P. Tinnefeld, “Photophysics of Fluorescent Probes for Single-Molecule Biophysics and Super-Resolution Imaging,” *Annu. Rev. Phys. Chem.*, vol. 63, no. 1, pp. 595–617, May 2012.

[118] D. Landgraf, B. Okumus, P. Chien, T. A. Baker, and J. Paulsson, “Segregation of molecules at cell division reveals native protein localization,” *Nat. Methods*, vol.

9, no. 5, pp. 480–482, May 2012.

[119] E. Lang, J. Baier, and J. Köhler, “Epifluorescence, confocal and total internal reflection microscopy for single-molecule experiments: a quantitative comparison,” *J. Microsc.*, vol. 222, no. 2, pp. 118–123, May 2006.

[120] M. J. Sanderson, I. Smith, I. Parker, and M. D. Bootman, “Fluorescence Microscopy,” *Cold Spring Harb. Protoc.*, vol. 2014, no. 10, pp. 1–36, Oct. 2014.

[121] M. M. Frigault, J. Lacoste, J. L. Swift, and C. M. Brown, “Live-cell microscopy - tips and tools,” *J. Cell Sci.*, vol. 122, no. 6, pp. 753–767, Mar. 2009.

[122] F. Zernike, “Phase contrast, a new method for the microscopic observation of transparent objects,” *Physica*, vol. 9, no. 7, pp. 686–698, Jul. 1942.

[123] F. Zernike, “How I discovered phase contrast,” *Science.*, vol. 121, pp. 345–349, 1955.

[124] D. B. Murphy, R. Oldfield, S. Schwartz, and M. W. Davidson, “Introduction to Phase Contrast Microscopy | MicroscopyU,” *MicroscopyU*. [Online]. Available: https://www.microscopyu.com/techniques/phase-contrast/introduction-to-phase-contrast-microscopy. [Accessed: 16-May-2019].

[125] N. S. M. Goncalves, S. Startceva, C. S. D. Palma, M. N. M. Bahrudeen, S. M. D. Oliveira, and A. S. Ribeiro, “Temperature-dependence of the single-cell variability in the kinetics of transcription activation in Escherichia coli,” *Phys. Biol.*, vol. 15, no. 2, p. 026007, 2018.

[126] A. S. Ribeiro, “Laboratory for single cell biology studies of the LBD.” [Online]. Available: https://sites.google.com/view/andreribeirolab/home/laboratory?authuser=0. [Accessed: 15-May-2019].

[127] L. Martins, R. Neeli-Venkata, S. M. D. Oliveira, A. Häkkinen, A. S. Ribeiro, and J. M. Fonseca, “SCIP: a single-cell image processor toolbox,” *Bioinformatics*, vol. 34, no. 24, pp. 4318–4320, 2018.

[128] A. Häkkinen, A. Muthukrishnan, A. Mora, J. M. Fonseca, and A. S. Ribeiro, “CellAging: a tool to study segregation and partitioning in division in cell lineages of Escherichia coli,” *Bioinformatics*, vol. 29, no. 13, pp. 1708–1709, 2013.

[129] A. D. Mora, P. M. Vieira, A. Manivannan, and J. M. Fonseca, “Automated drusen detection in retinal images using analytical modelling algorithms,” *Biomed. Eng. Online*, vol. 10, no. 1, p. 59, 2011.

[130] A. Hakkinen and A. S. Ribeiro, “Estimation of GFP-tagged RNA numbers from temporal fluorescence intensity data,” *Bioinformatics*, vol. 31, no. 1, pp. 69–75, Jan. 2015.

[131] M. Zare, R. Neeli-venkata, L. Martins, S. Peltonen, U. Ruotsalainen, and A. S. Ribeiro, “Automatic Classification of Z-ring Formation Stages at the Single Cell Level in Escherichia Coli by Machine Learning Automatic Classification of Z-ring Formation Stages at the Single Cell Level in Escherichia Coli by Machine Learning,” in *4th International Conference on Bioimaging (BIOIMAGING 2017)*, 2017.

[132] P. Ruusuvuori *et al.*, “Evaluation of methods for detection of fluorescence labeled subcellular objects in microscope images,” *BMC Bioinformatics*, vol. 11, no. 1, p. 248, Dec. 2010.